Hindawi
Shock and Vibration
Volume 2017, Article ID 1205976, 34 pages
https://doi.org/10.1155/2017/1205976

Research Article

Wind-Induced Coupling Vibration Effects of High-Voltage Transmission Tower-Line Systems

Meng Zhang,[1] Guifeng Zhao,[1] Lulu Wang,[1] and Jie Li[2,3]

[1]*School of Civil Engineering, Zhengzhou University, Zhengzhou 450001, China*
[2]*College of Civil Engineering, Tongji University, Shanghai 200092, China*
[3]*State Key Laboratory for Disaster Reduction in Civil Engineering, Tongji University, Shanghai 200092, China*

Correspondence should be addressed to Guifeng Zhao; gfzhao@zzu.edu.cn

Received 27 July 2017; Accepted 24 October 2017; Published 10 December 2017

Academic Editor: Xing Ma

A three-dimensional finite element model of a 500 kV high-voltage transmission tower-line coupling system is built using ANSYS software and verified with field-measured data. The dynamic responses of the tower-line system under different wind speeds and directions are analyzed and compared with the design code. The results indicate that wind speed plays an important role in the tower-line coupling effect. Under the low wind speed, the coupling effect is less obvious and can be neglected. With increased wind speed, the coupling effect on the responses of the tower gradually becomes prominent, possibly resulting in the risk of premature failure of the tower-line system. The designs based on the quasi-static method stipulated in the current design code are unsafe because of the ignorance of the adverse impacts of coupling vibration on the transmission towers. In practical engineering, when the quasi-static method is still used in design, the results for the design wind speed should be multiplied by the corresponding tower-line coupling effect amplifying coefficient δ.

1. Introduction

High-voltage transmission tower-line systems are important lifeline engineering infrastructures, which are vital to the harmony and sustainable development of society. A high-voltage transmission tower-line system is composed of the transmission towers and transmission lines with a large difference in stiffness between them. Because of their characteristics, including their geometric nonlinearity and closely spaced modes of vibration, the dynamic behavior of transmission lines has significant effects on the wind-induced vibration response of transmission towers. Damage to high-voltage overhead transmission lines caused by environmental impacts, especially by wind-induced vibration, has been an important issue for engineers and researchers in the power industry throughout the world [1–8]. Since the introduction of the first high-voltage transmission lines, this issue has been studied continually, but reasonable solutions have not yet been obtained. Transmission line damage caused by strong winds (the average wind speed at a height of 10 m is greater than 10.8 m/s, corresponding to a Beaufort number greater than 6) still frequently happens. In Argentina, Australia, Brazil, Canada, Japan, South Africa, and the United States, more than 80% of the transmission lines damage in these countries is caused by extreme winds [9]. For example, in September 1961, Hurricane Carla caused over $1.5 million in damage to utility companies in Houston, USA [10]. In September 1989, Hurricane Hugo seriously damaged the power lines from Guadeloupe Island to Virginia, USA. The most severely affected area was the Montserrat region, where all high-voltage and low-voltage transmission lines were destroyed by the hurricane [11]. On October 1, 2002, typhoon number 21 landed in Japan and caused severe accidents, leading to the collapse of the 10 high-voltage transmission towers in Ibaraki prefecture [2]. In 2005, Hurricane Katrina landed in the United States and caused outages to 2.9 million customers. Hurricane Wilma also caused 6 million customers to lose power supply [2]. On November 10, 2009, a severe thunderstorm hit the transmission lines in southern Brazil, which resulted in the collapse of three transmission lines connecting the Itaipu hydropower station to Sao Paulo, causing power outages across large areas; more than 60 million people

were affected in 12 states in Brazil [12]. China's situation is not better. From 1988 to 2009, more than 105,500 kV high-voltage transmission lines collapsed [2, 3]. Therefore, wind-induced failure of high-voltage transmission line structures has been a common issue around the world. The problems uncovered by the above-mentioned accidents are profound warnings to the power sector and national security agencies throughout the world.

Researchers in China and other countries have performed experimental research and theoretical analysis regarding the wind-induced dynamic response of high-voltage transmission tower-line coupling systems. Using aeroelastic wind tunnel models, the experimental studies have focused on the wind-induced response characteristics of tower-line coupling systems [13–19], aerodynamic damping of wires [20], dynamic tension of ice-covered wires [21], and wind-induced responses in ice-covered line structures [22–26]. Researchers have also conducted field dynamic measurement studies of transmission line structure [27–32], but due to field test conditions, the existing field tests have mostly focused on the dynamic characteristics of transmission tower structure [27–30]. The existing field measurement studies regarding wind-induced responses of tower-line coupling systems are still insufficient. At present, finite element analysis is the most frequently used method for theoretical analysis of wind-induced vibration responses of transmission tower-line coupling systems because, compared with wind tunnel tests and field measurement technology, finite element analysis not only considers the coupling vibration effect between transmission towers and cables but also better characterizes the geometric nonlinear vibration in transmission lines. Moreover, finite element analysis can be used to conveniently analyze the wind-induced vibration responses of transmission tower-line systems under different wind speeds. For these reasons, finite element analysis has been widely used in the study of wind-induced vibration of transmission line structures [33–37]. However, because the test data and the measured field wind-induced response data are limited, the applicability of finite element analysis models for tower-line systems has not been validated. Therefore, building reliable finite element analysis models for high-voltage transmission tower-line coupling systems is a common goal.

Due to the increase in power demand worldwide, the voltage levels of transmission lines continue to increase. Transmission tower-line systems have gradually been developed to use larger spans and higher overhead hanging structures, and thus the wind-induced vibration effect of the transmission lines has become even more prominent. In contrast, because of the frequent occurrence of extreme winds associated with global climate change, the probabilities of large-scale power outages caused by transmission line trips and tower collapses under strong winds are further increasing. Therefore, it is especially important to conduct detailed dynamic analysis and design of transmission lines to ensure that transmission towers can operate safely within their design service periods.

At present, the design of transmission tower-line structures as stipulated in the current codes of most countries requires that transmission towers and transmission lines to be designed separately. The adverse impacts of coupling vibration on the transmission towers in tower-line systems under the design wind loadings are not considered. Under the action of fluctuating wind loads, the dynamic tension of the transmission lines will change continuously, which may cause the forces of the transmission tower members to be in a complex stress state and may cause the members to yield before their designed bearing capacity is reached, due to dynamic characteristics and failure mode of the tower changed. Furthermore, the dynamic characteristics and failure modes [38] of the tower are changed. Therefore, the study of the coupled vibration behavior of high-voltage transmission tower-line systems under wind load is of great theoretical significance. At the same time, it can provide guidance for the design of transmission line structures.

In recent years, researchers have realized that the effects of coupling between the towers and lines in transmission tower-line systems on the dynamic response of the transmission towers cannot be neglected. It has been suggested that the disadvantage effect of the coupling between the towers and lines should be considered when designing transmission line structures. However, studies of the specific characteristics and influence of the coupling vibration responses of tower-line systems under wind load remain limited.

To address the topics discussed above, in this study, using a 500 kV high-voltage transmission tower-line system in East China as an engineering example, a finite element analysis model matching the practical tower-line system is developed. Based on the wind speed and pressure conversion theory, the wind speeds recorded on the transmission lines are converted into wind loads. A finite element analysis of the wind-induced vibration response of the tower-line system is conducted. The results are compared with the measured data to verify the accuracy of the finite element model of the transmission tower-line system. On this basis, using the modified Davenport spectrum to simulate the wind speed time history, the dynamic responses of the transmission towers in the tower-line system under different wind speeds are analyzed. The results are compared with those provided by the static calculation method stipulated in China's "Technical Codes for Designing 110 kV–750 kV Overhead Transmission Lines" (GB50545-2010) [39]. Based on the results of this analysis, the ratio of the tower members' stress in the tower-line system to the quasi-static stress of the members of a single tower is defined as the tower-line coupling effect amplifying coefficient, δ. The variation in this coefficient under different wind speeds and directions is discussed. A quantitative design methodology is proposed. The purpose of this study is to provide technical support for the wind resistance design of high-voltage transmission tower-line systems.

2. Finite Element Model of High-Voltage Transmission Tower-Line Systems

2.1. Engineering Background and Calculation Parameters. The 500 kV high-voltage transmission line in this study is located in Jiangsu Province, China. Along the transmission line, a tower-line system consisting of 3 transmission towers (towers numbers 159, 160, and 161) and 2-span transmission lines were selected for this study, as shown in Figure 1. Transmission

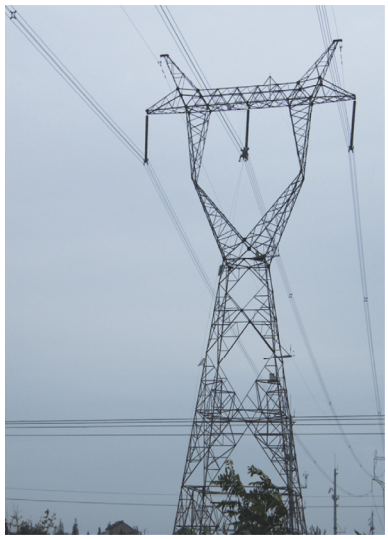

Figure 1: A high-voltage transmission tower-line system (tower number 160).

tower number 160 has a height of 47.1 m with cross arm 42 m above ground. The spacing between the middles of number 159 and number 160, crossing a flat field, is 280 m, and the spacing between the middles of number 160 and number 161, crossing a river with complex terrain, is 380 m. The transmission lines are in two layers. The upper layer is the lightning wires, and the lower is the electric conductors. Between number 159 and number 160, the maximum sags of the lightning wires and electric conductors are 4.3 m and 5.6 m, respectively, whereas between number 160 and number 161, the maximum sags of the lightning wires and electric conductors are 7.92 m and 10.32 m, respectively.

The transmission towers are angle steel towers. Their main members, model, and locations are shown in Table 1. The main members are Q345 steel, whereas the oblique members are Q235. The design parameters of the transmission lines are shown in Table 2. One end of the porcelain insulators is hinged at the end of the conductors. The other end is hinged in the cross arm of the tower. Three umbrella-shaped hanging insulator strings are used. Each string is composed of 27 pieces, with each piece weighing 12.0 kg. The total length of string is 4 m, the diameter is 330 mm, and the total weight is 370.29 kg.

The average wind speed at a height of 10 m is 25.3 m/s. This is used as the design wind resistance condition for these transmission lines.

2.2. The Establishment of the Finite Element Analysis Model. To accurately calculate the wind-induced vibration response of the transmission tower-line system, a precise and reasonable finite element model of the multi-tower-line coupled system is required. Zhang [40] numerically studied the finite element modeling of transmission tower-line systems using the ANSYS software package and compared the wind-induced vibration responses of a four-tower three-wire system with those of a three-tower two-wire system. The results indicate

Table 1: Parameters of the main members of the transmission towers.

Number	Members specification	Applications in the tower
(1)	L180 × 16	Junction connecting insulator and crossbar, ground bracket
(2)	L100 × 10	Low crank arm in tower head
(3)	L100 × 8	Tower and tower legs (bottom)
(4)	L90 × 8	Tower head
(5)	L90 × 7	Tower oblique members, upper crank arm in tower
(6)	L80 × 7	Cross arm
(7)	L80 × 6	Tower head, crossbars; tower oblique members
(8)	L70 × 5	Oblique members, connector between tower head and crossbars
(9)	L63 × 5	Tower head, tower oblique members
(10)	L56 × 5	Tower oblique members, tower head bracing
(11)	L50 × 5	Tower bracing
(12)	L45 × 5	Tower legs (bottom), tower bracing

that the three-tower two-line model can meet the accuracy requirements for calculation with the lower computational cost. Therefore, in this study, the ANSYS software package is still used to establish the spatial finite element analysis model for the three-tower two-line system based on the actual characteristics of the transmission lines.

In the model, the angle steel member in the transmission tower is simulated using the BEAM24 element. This element is a three-dimensional thin-walled plastic beam element. All cross-sections of the beam have tensile, bending, and torsion bearing capabilities, and the model can simulate the beam element with any openings. The element has plastic, creep, and expansion bearing capacities in the axial and customized cross-section opening directions. The material of the element is simulated based on a double linear model, as the elastic and plastic properties are accommodated simultaneously. The detailed materials parameters are as follows: before the yield, the elastic modulus is 2.06×10^5 MPa, the Poisson ratio is 0.3, and the design yield strength is 310 MPa (Q345 steel) or 215 MPa (Q235 steel). After the yield, the tangent modulus is 4120 MPa.

The transmission line is a typical type of suspended cable structure. Any given conductor (ground wire) with arbitrary deflection can be discretized into a series of interconnected cable elements. After the discretization, the span-to-sag ratio of each cable element is less than that of the original cable. Therefore, the small deflection cable theory can be used to analyze each cable element. There are generally two methods currently in use to simulate the cable element. In one approach, the cable element is regarded as a straight bar with only a tensile force, and all the loads act on the nodes. This method is comparatively simple and will work accurately only when the cable pretension is far greater than the tension caused by cable deadweight (i.e., the span-to-sag ratio of the

Table 2: Design parameters of the transmission lines.

Item	Diameter d (mm)	Cross sectional area A_c (mm^2)	Line density m_c (kg/m)	Elastic modulus E_c (MPa)	Average operating tension (N)	Tension under design wind speed (N)	Rupture force (N)	Span L_c (m)	Sag d_c (m)
Electric conductor	33.6	666.55	2.06	63000	35316	43688	141265	280 (380)	5.6 (10.32)
Lightning wire	16	152.81	0.639	91100	14275	21929	79306	280 (380)	4.3 (7.92)

Table 3: Parameters of the transmission lines after equivalent processing.

Items	Diameter d (mm)	Density ρ_c (kg/m^3)	Line density m_c (kg/m)	Linear load q_c (N/m)	Initial strain ε_{c0}
Electric conductor	134.4	3090.5	8.24	80.752	0.00084
Lightning wire	16	4182	0.639	6.262	0.0010254

cable element is sufficiently small, often less than 1/12). The other method is to consider each cable element as a parabolic cable element, assuming that the vertical load (including the deadweight) is evenly distributed along the cable span. Similarly, this method also requires a small rise-to-span ratio of the cable element, usually less than 1/8. Considering that the maximum span sag ratio (d_c/L_c) of the transmission line in this study is approximately 1/37, much less than 1/12, we chose the first method to model the transmission line using the LINK10 element. Each element covers 1 m of length. This element can simulate rod members under axially applied tension or compressive loadings, and it can also be used to simulate relaxed suspension or chain structures. This element also has stress stiffening and geometric nonlinear analysis capabilities and can therefore meet the requirements of model building for transmission lines. The cable span between the middles of number 159 and number 160 is discretized into 280 LINK10 elements, and the cable span between the middles of number 160 and number 161 is discretized into 380 LINK10 elements. Compared with the other studies (see Gani and Légeron [34] and Fei et al. [41]), the mesh is comparatively intensive.

In practical transmission lines, each phase wire is composed of four-split wires; to simplify the calculations, in the finite element analysis model, each four-split phase wire is simplified as one piece of wire, assuming each split wire has the same windward cross-section, and thus, the operating tension of this piece of wire should be equivalent to the total operating tension, and its density should be equivalent to the averaged density of each split. The parameters of this simplified transmission line are presented in Table 3.

When establishing the finite element model of the transmission line, it is very important to determine its initial configuration. On the one hand, the balance equation and the deformation coordination equation of the transmission line should be determined based on the catenary theory, to determine the spatial location of the transmission line. On the other hand, it is necessary to transfer the transmission line from the initial stress-free state to the initial load state in accordance with certain shape-determining methods. The main methods for determining the cable balance equation are the catenary theory method and the parabolic theory method. The former is an exact method, whereas the latter is an approximate method, but when the span-to-sag ratio of the cable is less than 1/8, the parabolic theory method also provides a relatively accurate solution. Because the maximum span sag ratio (d_c/L_c) of the transmission line in this study is approximately 1/37, much less than 1/8, the parabolic method can be used to determine the initial shape of the transmission line. Assuming that the vertical load on the transmission line is evenly distributed along the span, as shown in Figure 2, the spatial shape equation of the transmission line is

$$y(z) = \frac{q_c}{2T_{c0}} z\left(L_c - z\right) + \frac{\Delta_c}{L_c} z. \tag{1}$$

In (1), q_c is the vertical load applied on the transmission line, with only the transmission line's own weight being considered in this study; T_{c0} is the initial horizontal tension of the transmission line, $T_{c0} = (q_c L_c^2)/(8d_c)$; L_c is the horizontal span of the transmission line (half the distance between the two adjacent towers); Δ_c is the height difference between the two ends of the transmission line; and d_c is the sag in the middle of the transmission line. Using the parameters listed in Tables 2 and 3, the spatial shape equation can be determined. The initial strain that always exists in the transmission line results in the existence of the initial stress and the initial tension within the system. Therefore, the shape-determining analysis is conducted on the wire element when the finite element model is built. The purpose is to establish the initial stress state to ensure that the subsequent analysis results are correct.

The insulator is simulated with the rigid element MPC184, with rigid rod properties to simulate the spatial rigid body motion of the insulator. This choice is made because the porcelain insulator has higher stiffness than the transmission lines. The MPC184 element can be used to model a rigid constraint between two deformable bodies or as a rigid component used to transmit forces and moments in engineering

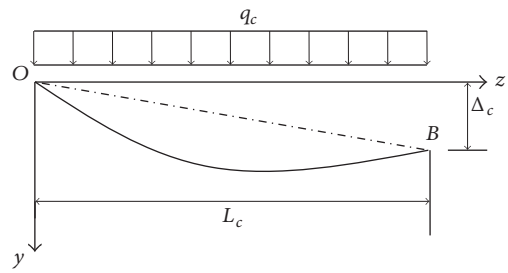

Figure 2: Diagram of evenly distributed vertical loadings along the span of the transmission line.

applications. This element is well suited for linear, large-rotation, and/or high-strain nonlinear applications.

To simplify the analysis, the model of the three transmission towers is built based on the parameters of tower number 160. The three-dimensional finite element models of the single tower and the tower-line coupling system are shown in Figure 3. In the model, the four nodes at the bottom of each transmission tower are rigidly constrained, and the displacement constraints in the Z coordinate direction are imposed on the connecting junctures between the transmission lines and the transmission tower. The single tower model has 1971 elements and 839 nodes in total, whereas the tower-line system model has 9210 elements and 5972 nodes in total, with 25936 degrees of freedom.

3. Analysis of the Free Vibration of the Transmission Tower-Line System

In the transmission tower-line coupling system, the tower and the line work together. The basic dynamic characteristics of the tower-line system can be obtained based on modal analysis. The dynamic characteristics include the vibration mode and frequency. Through modal analysis, the vibration response of the system when subjected to external excitation can be predicted.

The free vibrations of the transmission tower and the tower-line system discussed above are analyzed individually using the finite element model. The initial 300 orders of the natural frequency of the tower-line coupling system and the corresponding vibration modes are analyzed. The first 5 orders in the results are the rigid body motion of the insulator in the system, whose natural frequency is close to zero. Then, orders 6 to 15 are the vibration of the transmission lines, whose natural frequency is between 0.232 and 0.323 Hz. The 16th, 17th, 19th, 40th, 112th, 119th, 120th, 128th, and 161st orders represent the overall vibration model of the tower-line coupling system. The results of the rest of the higher-order vibration modes are not listed. Among the vibration models, the 16th-order mode mainly represents the vibration of the lightning wires and of the transmission towers along the z-direction (Figure 4(a)), with a corresponding frequency of 0.38 Hz. The 17th-order vibration mode is the torsion vibration of the lightning wires and of the transmission towers (Figure 4(b)), with a corresponding frequency of 0.39 Hz. The 19th-order vibration mode is the vibration of the transmission lines and the torsion vibration of the transmission towers (Figure 4(c)), with a corresponding frequency of 0.467 Hz. The 40th-order vibration mode also represents the torsion vibrations of the tower-line transmission lines and the transmission towers (Figure 4(d)), with a corresponding frequency of 0.724 Hz. The 112th-vibration mode is the vibration of the transmission lines and of the transmission towers along x-direction (Figure 4(e)), with a corresponding frequency of 2.228 Hz. The 119th-order vibration mode also represents the vibration of the power transmission lines and of the transmission towers along the x-direction (Figure 4(f)), with a corresponding frequency of 2.295 Hz. The 120th-order vibration mode is the vibration of the transmission lines and the transmission towers along the z-axis (Figure 4(g)), with a corresponding frequency of 2.318 Hz. The 128th-order vibration mode is the vibration of the transmission lines and transmission towers along the x-direction (Figure 4(h)), with a corresponding frequency of 2.384 Hz. The 161st-order vibration mode is the vibration of the transmission lines and the torsion vibration of the transmission towers (Figure 4(i)), with a corresponding frequency of 3.138 Hz.

The results for the natural frequencies and characteristics of the vibration modes of the tower-line system are listed in Table 4. When the tower-line coupling system is vibrating as a whole, the dynamic characteristics of the transmission tower are pronouncedly different from that of an individual single transmission tower. The natural frequency of the transmission tower in the tower-line coupling system is much lower than that of the individual single tower in the corresponding vibration direction. In the tower-line system, the vibration of the transmission tower in the z- and torsion directions is more prone to occur at low frequencies, whereas the vibration in the x-direction still occurs at high frequencies. In the tower-line system, the overall vibration of the tower and the line is characterized by low-frequency, dense-mode vibration, which is different from the vibration characteristics of a single tower, demonstrating that, in the design of transmission tower-line structures, the tower-line coupling effect on the dynamic characteristics of transmission tower should be considered.

4. Comparison of Field Measurements and Finite Element Simulation of the Wind-Induced Vibration Response of the Transmission Tower-Line System

4.1. Introduction to the Field Measurements. The anemometers are placed at vertical heights of 10, 20, 28, and 43 m on tower number 160 to record the wind speed on the different parts of the transmission tower. Three wind towers were installed between transmission towers number 159 and number 160. Two ultrasonic anemometers are installed on each wind tower at heights of 10 m and 20 m. The 1st wind tower is 40 m from transmission tower number 160, the 2nd wind tower is 80 m from the 1st wind tower, and the 3rd wind tower is 120 m from the 2nd wind tower and 40 m from transmission tower number 159. The layout diagram of all wind instruments is shown in Figure 5. The acceleration sensors

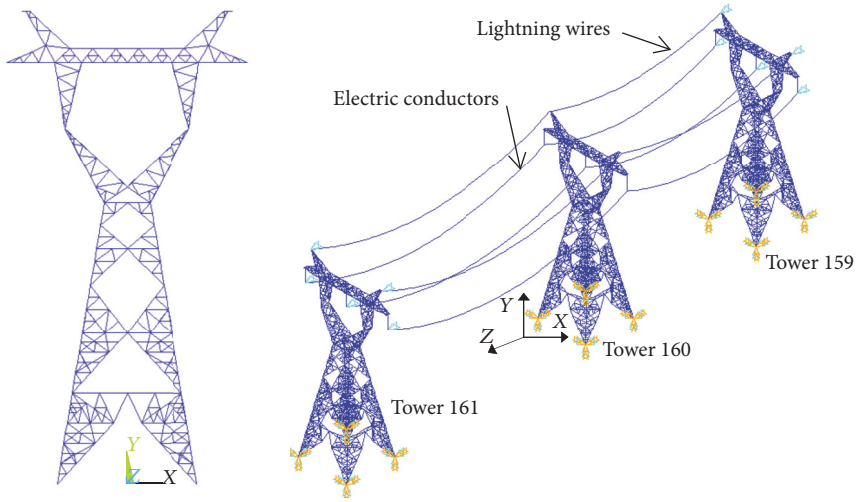

(a) Tower number 160 (b) Tower-line system

Figure 3: Finite element analysis model of the high-voltage transmission tower-line system.

Table 4: Comparison of the natural frequencies of the transmission tower-line system and a single transmission tower.

Model	Natural frequency of the transmission tower in tower-line system (Hz)	Characteristics of the vibration of the transmission tower in tower-line system	Natural frequency of a single tower (Hz)	Characteristics of the vibration of a single tower
(1)	0.38	Bending vibration in the z-direction	1.7497	Bending vibration in the z-direction
(2)	0.39	Torsion vibration	2.1481	Bending vibration in the x-direction
(3)	0.467	Torsion vibration	2.8720	Torsion vibration
(4)	0.724	Torsion vibration	4.1825	Local vibration in the tower
(5)	2.228	Vibration in the x-direction	5.0337	Coupling vibration in the z-direction and the tower's local vibration

are mounted vertically at different heights on tower number 160, noted as locations A, B, C, and D in Figure 5(a). When conducting the field measurements, the sampling frequency of the anemometers is 10 Hz, and the sampling frequency of the acceleration sensors is 100 Hz. A total of 165 seconds of acceleration response were recorded for each sample.

In September 2007, when Typhoon Wipha hit East China, the measuring equipment discussed above successfully recorded the wind speed in these locations and the acceleration response of transmission tower number 160 under the effects of the typhoon. Typhoon Wipha's strength attenuated quickly after landfall. Therefore, the average field wind speeds at heights of 10, 20, and 28 m were 6.03, 7.43, and 8.13 m/s, respectively. Figure 6 shows a dataset of wind speed time history recorded by the anemometers at 10 and 20 m on transmission tower number 160. Figure 7 shows the fluctuating wind speed power spectrum density (PSD) recorded by anemometers at 20 m on the transmission tower and on the wind tower.

4.2. Calculation of the Wind Load on Various Locations of the Measured Transmission Lines. To provide the basis for the finite element simulation of the wind-induced vibration response of the measured transmission lines, the wind speed recorded in the field must be converted into the wind loads on the lines. When calculating the wind loads on the measured transmission lines for transmission tower number 160, considering the influence of the change of wind speed along the height of the transmission tower, as shown in Figure 8, the tower can be divided into eight sections vertically. The wind speed recorded by the anemometer at a height of 43 m is selected as the wind speed for sections 1 to 3, that at a height of 28 m is used for sections 4 and 5, that at a height of 20 m is used for section 6, and that at 10 m is employed for sections 7 and 8.

The wind loadings on the transmission lines should be calculated separately in accordance with the actual layout of the anemometers and wind towers. Because the three wind towers are installed between transmission towers number

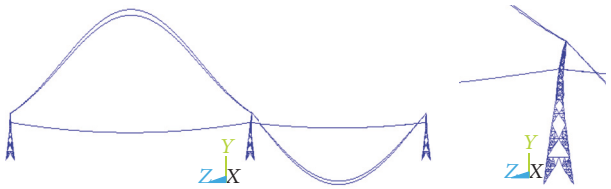

Overall side view | Side view of tower number 160

(a) The 1st-order vibration mode in the tower-line system in the z-direction (the 16th-order, $f = 0.38$ Hz)

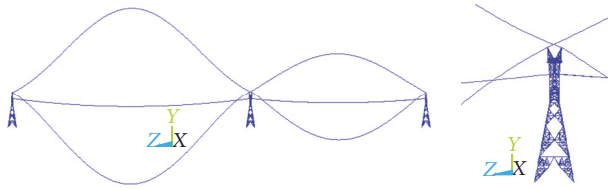

Overall side view | Side view of tower number 160

(b) The 1st-order vibration mode in the tower-line system in the torsion direction (the 17th-order, $f = 0.39$ Hz)

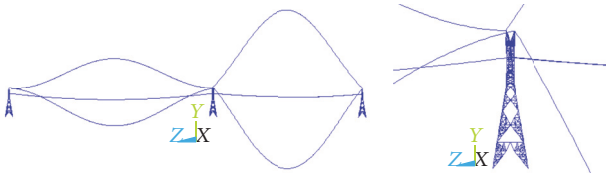

Overall side view | Side view of tower number 160

(c) The 2nd-order vibration mode in the tower-line system in the torsion direction (the 19th-order, $f = 0.467$ Hz)

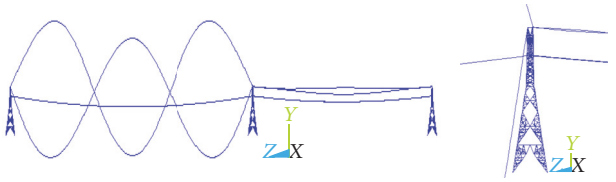

Overall side view | Side view of tower number 160

(d) The 3rd-order vibration mode in the tower-line system in the torsion direction (the 40th-order, $f = 0.724$ Hz)

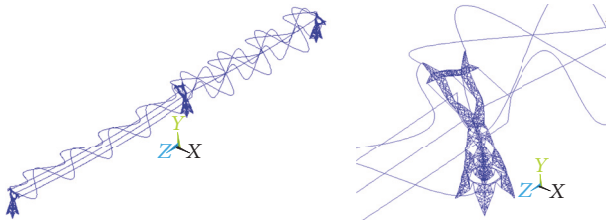

Overall side view | Side view of tower number 160

(e) The 1st-order vibration mode in the tower-line system in the x-direction (the 112th-order, $f = 2.228$ Hz)

Overall side view | Side view of tower number 160

(f) The 2nd-order vibration mode in the tower-line system in the x-direction (the 119th-order, $f = 2.295$ Hz)

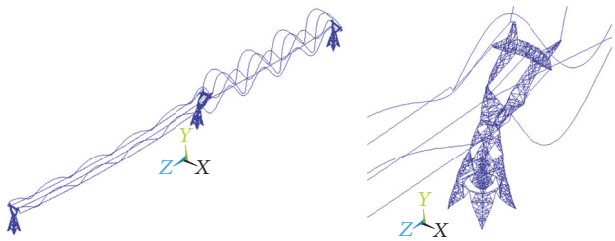

Overall side view | Side view of tower number 160

(g) The 2nd-order vibration mode in the tower-line system in the z-direction (the 120th-order, $f = 2.318$ Hz)

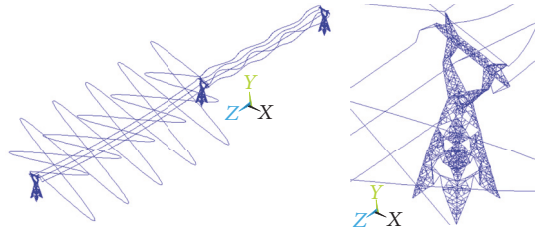

Overall side view | Side view of tower number 160

(h) The 3rd-order vibration mode in the tower-line system in the x-direction (the 128th-order, $f = 2.384$ Hz)

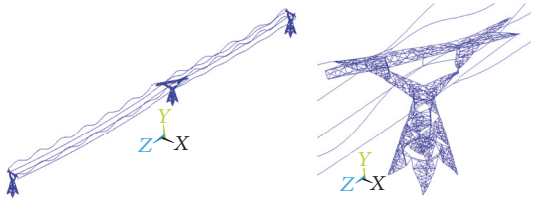

Overall side view | Side view of tower number 160

(i) The 4th-order vibration mode in the tower-line system in the torsion direction (the 161st-order, $f = 3.138$ Hz)

Figure 4: Vibration modes of the transmission tower-line system.

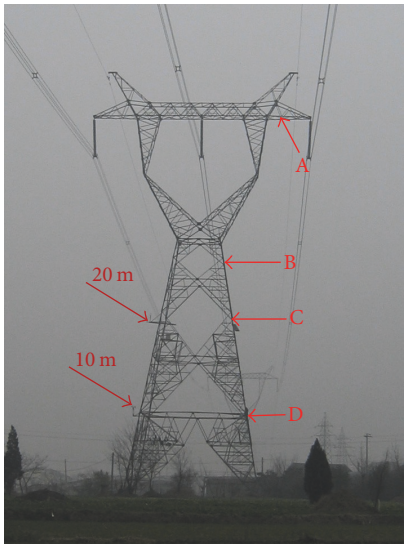

(a) The placement locations of the anemometers and acceleration sensors on tower number 160

(b) The placement of the wind tower and anemometers

(c) The anemometers on transmission tower number 160

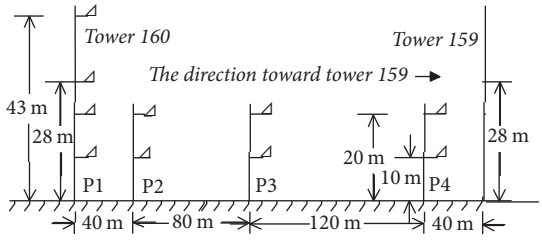

(d) Diagram of the anemometer installation locations (note: the symbol "⊿" represents a three-dimensional ultrasonic anemometer)

Figure 5: Arrangements of wind instruments and acceleration sensors in the field.

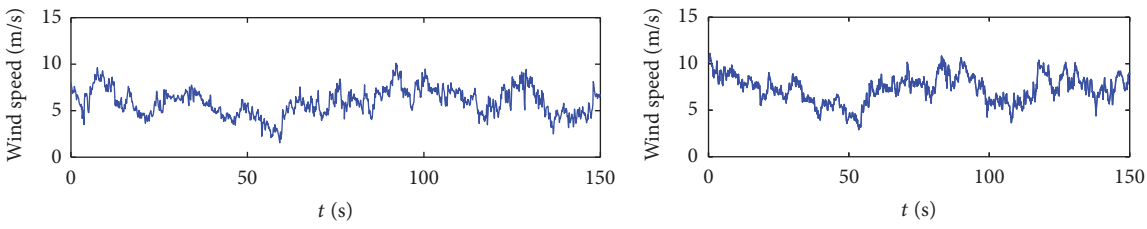

(a) Wind speed time history at a height of 10 m

(b) Wind speed time history at a height of 20 m

Figure 6: Wind speed data recorded by the anemometers on tower number 160.

160 and number 159, as shown in Figure 5, this span of the transmission lines can be divided into four sections from tower number 160 to tower number 159, and the wind loading can then be calculated section by section. Among them, the wind speed recorded by the anemometers at a height of 43 m on tower number 160 is used as the wind speed for the 1st section and that at a height of 20 m on the 1st wind tower is used for the 2nd section; the speed at a height of 20 m on the 2nd wind tower is employed for the 3rd section and that at a height of 20 m on the 3rd wind tower is used for the 4th section. For the transmission lines between transmission towers number 160 and number 161, no wind-measuring devices are installed because of the watercourse between them and the complex terrain conditions. When calculating

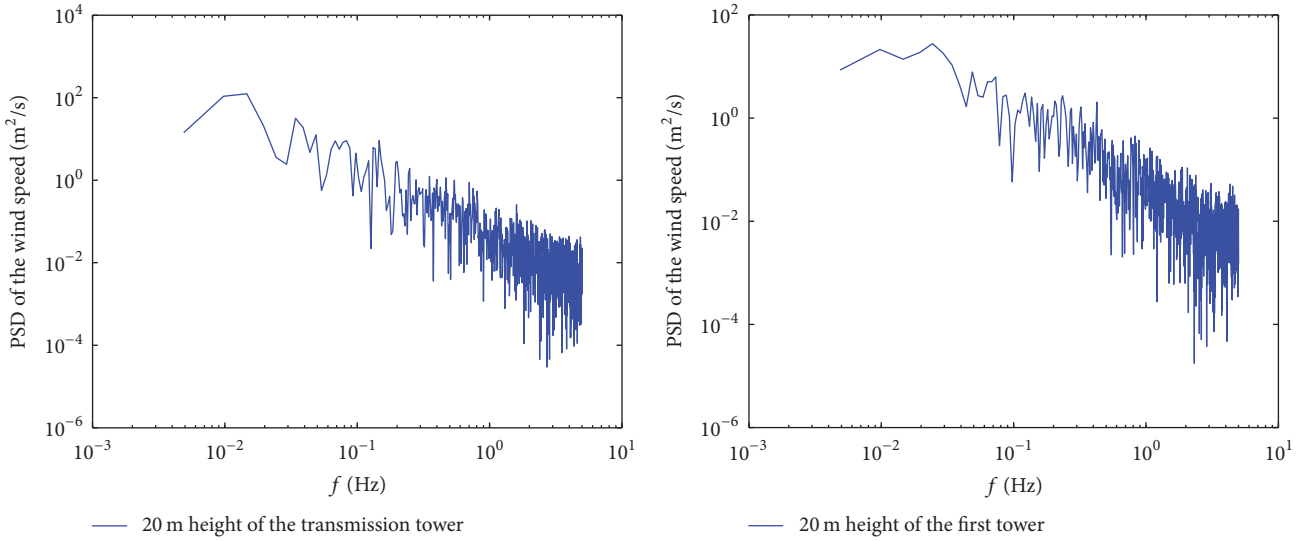

(a) Wind speed PSD at a height of 20 m on transmission tower number 160

(b) Wind speed PSD at a height of 20 m on the 1st wind tower

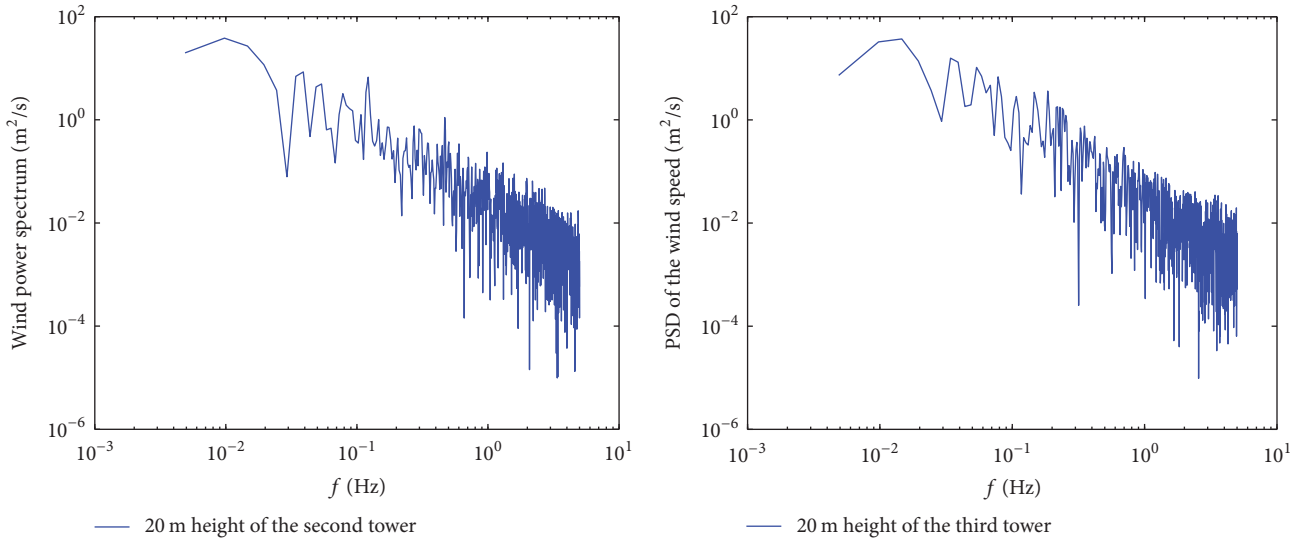

(c) Wind speed PSD at a height of 20 m on the 2nd wind tower

(d) Wind speed PSD at a height of 20 m on the 3rd wind tower

Figure 7: The fluctuating wind speed PSD recorded by the anemometers at each field measuring location of the transmission lines.

the wind loadings on the transmission lines in this section, the wind speed recorded by the anemometers at a height of 43 m on transmission tower number 160 is used.

The wind load applied on the insulators can be calculated based on the wind speed recorded at the corresponding height on the transmission towers.

In the matrix of field wind-measuring devices, every anemometer can record the wind speed in the main direction, the wind speed perpendicular to the main direction, and the vertical wind speed at its location. Under normal circumstances, the wind speed in the main direction is much greater than the speeds in the perpendicular and vertical directions. Considering that the transmission tower has a large stiffness, the focus should be on the impact of the horizontal wind speed, whereas the impact of vertical wind load can be neglected. For the relatively flexible transmission lines, the effects of both the horizontal and vertical wind loads should be considered. Because the angle between the actual measured direction of the dominant wind and that of the transmission lines is approximately 106°, the main dominant wind speed and the wind speed perpendicular to the dominant wind direction can be decomposed into the wind speed perpendicular to the line direction and the wind speed parallel to the line direction.

After obtaining the wind speed vector, the wind loading on a unit length of a slender structure can be calculated based on the method proposed by Dyrbye and Hansen [42]. The wind load $F(t)$ on the tower-line structure can be expressed as follows:

$$F(t) = \frac{1}{2}\rho\left(U(z) + u(z,t) - \dot{x}(z,t)\right)^2 B(z) C(z). \quad (2)$$

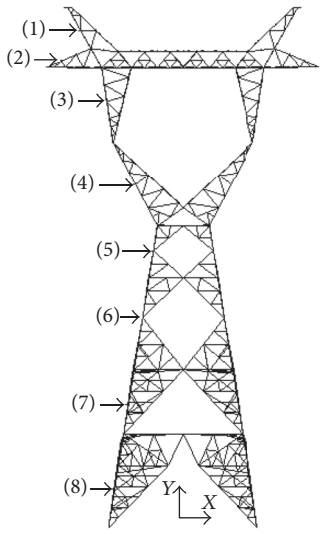

Figure 8: Vertical division of sections on transmission tower number 160.

In (2), ρ is the air density; $U(z)$ and $u(z,t)$ are the average wind speed and the fluctuating wind speed at height z, respectively; $\dot{x}(z,t)$ is the vibration velocity at height z; $B(z)$ is the height of the structure perpendicular to the wind direction; and $C(z)$ is the wind load shape coefficient of the structure at height z.

Equation (2) shows that the wind load on the structure depends on the aerodynamic coupling between the wind and the motion of the structure. To simplify the analysis, this study does not consider this coupling effect in the calculations. Therefore, the wind loading is calculated based on a quasi-steady hypothesis. Equation (2) can be simplified as follows:

$$F(t) = \frac{1}{2}\rho\left(U(z) + u(z,t)\right)^2 B(z) C(z). \tag{3}$$

In the detailed calculations, the wind loadings applied on the transmission towers and each section of the transmission lines can be calculated based on (3). When calculating the wind loads on the transmission towers, the towers' windward width can be calculated using its windward areas, A_s. The windward areas corresponding to each segment of transmission tower number 160 in Figure 8 are listed in Table 5.

4.3. Finite Element Simulation of the Wind-Induced Vibration Response of the Field-Measured Transmission Tower-Line System. The analysis of the wind-induced dynamic response of the transmission tower-line system can be summarized as the solutions to dynamic equations.

4.3.1. Principles of Calculation. Based on the finite element analysis method and the boundary conditions, the dynamic response of the actual transmission tower-line system can be expressed as the initial solutions of the discrete dynamic equations

$$[\mathbf{M}]\{\ddot{u}(t)\} + [\mathbf{C}]\{\dot{u}(t)\} + [\mathbf{K}]\{u(t)\} = \{\mathbf{F}(t)\}, \tag{4}$$

where [**M**], [**C**], and [**K**] are the structure's mass matrix, damping matrix, and stiffness matrix, respectively; $\{u(t)\}$, $\{\dot{u}(t)\}$ and $\{\ddot{u}(t)\}$ are the structure's displacement vectors, velocity vectors, and acceleration vectors, respectively; and $\{\mathbf{F}(t)\}$ is the wind's nodal load force vector.

The solution can be discretized in the time domain. The equation of motion can be divided into the equations of different discrete moments, and through stepwise integration, the responses of the structure in a series of discrete moments can be obtained. This method not only considers the nonlinear factors of the structure but also addresses the response of the different structural modes. Therefore, the calculation is highly accurate.

When calculating the damping of the transmission tower-line system, the Rayleigh damping matrix based on the orthogonal damping assumption is used. It is expressed as

$$[C] = \alpha[M] + \beta[K], \tag{5}$$

where α and β are the system's mass and stiffness coefficients, respectively. The equations are as follows:

$$\alpha = \frac{2\omega_i\omega_j\left(\xi_j\omega_i - \xi_i\omega_j\right)}{{\omega_i}^2 - {\omega_j}^2};$$
$$\beta = \frac{2\left(\xi_i\omega_i - \xi_j\omega_j\right)}{{\omega_i}^2 - {\omega_j}^2}. \tag{6}$$

In (6), ω_i and ω_j are system's ith-order and jth-order circular frequencies, and ξ_i and ξ_j are system's ith-order and jth-order damping ratios. As long as any two modes are determined, the coefficients α and β can be calculated.

Because the sampling frequency of the measuring anemometers in the field is 10 Hz and the corresponding wind speed recorded is 165 s, 1650 load steps are designed in the finite element analysis. The wind loads calculated for each section of the measured transmission lines are used as input for the finite element model. The wind-induced dynamic response of the tower-line coupling system is calculated using the implicit *Newmark-β* stepwise integration method. The geometrical nonlinearity of the transmission lines is considered in the calculation. To accurately obtain the high-order vibration response of the structure, 0.0025 s is selected as the integral time step, and 66000 loading substeps must be calculated.

4.3.2. Comparison of Finite Element (FE) Results and Field Measurement (FM) Values. Figure 9 shows a comparison of the finite element calculation results with the field measurement results at the locations A, B, C, and D on transmission tower number 160. The left side is a comparison of the acceleration time history, and the right side is a comparison of the acceleration PSD. By and large, the finite element calculation results are clearly in good agreement with the measured results. The calculated acceleration time history and the PSD at location A are in good agreement with the measured results. At locations B, C, and D, the acceleration time history results of the finite element analysis are in good agreement with the measured results. However, the acceleration PSD

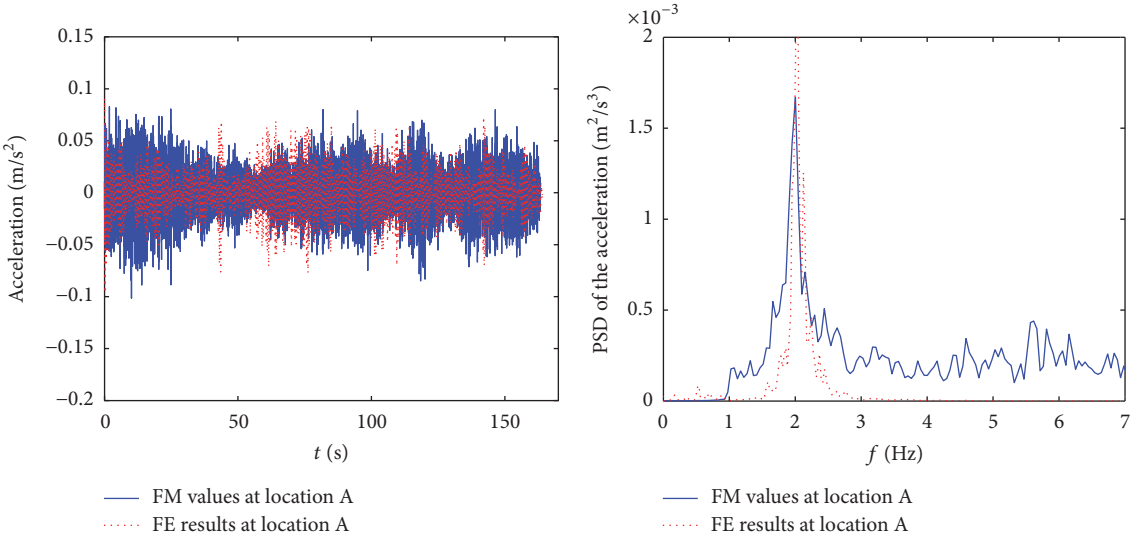

(a) Comparison of the acceleration time history at location A

(b) Comparison of the acceleration PSD at location A

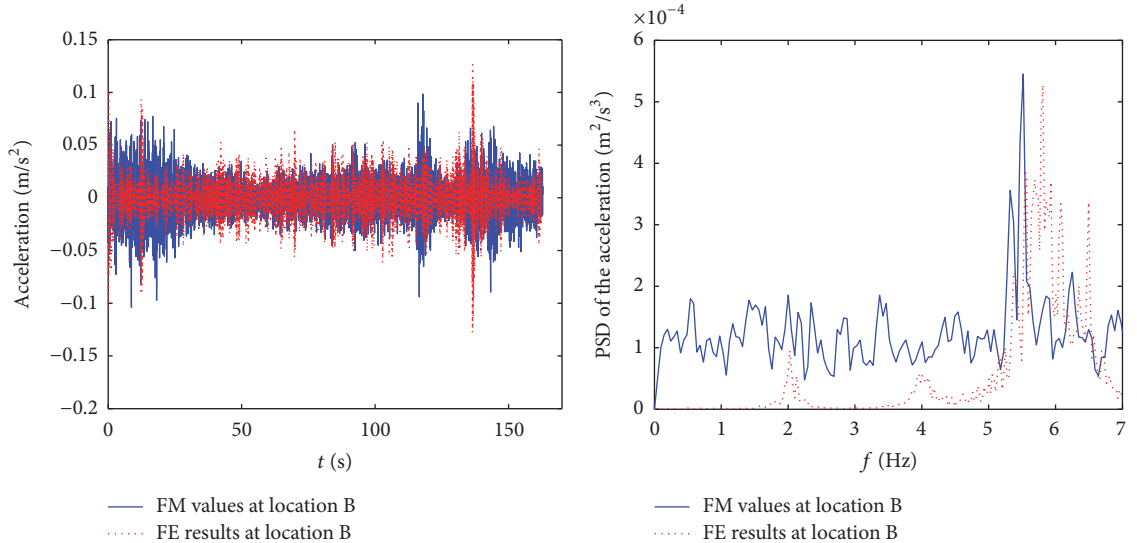

(c) Comparison of the acceleration time history at location B

(d) Comparison of the acceleration PSD at location B

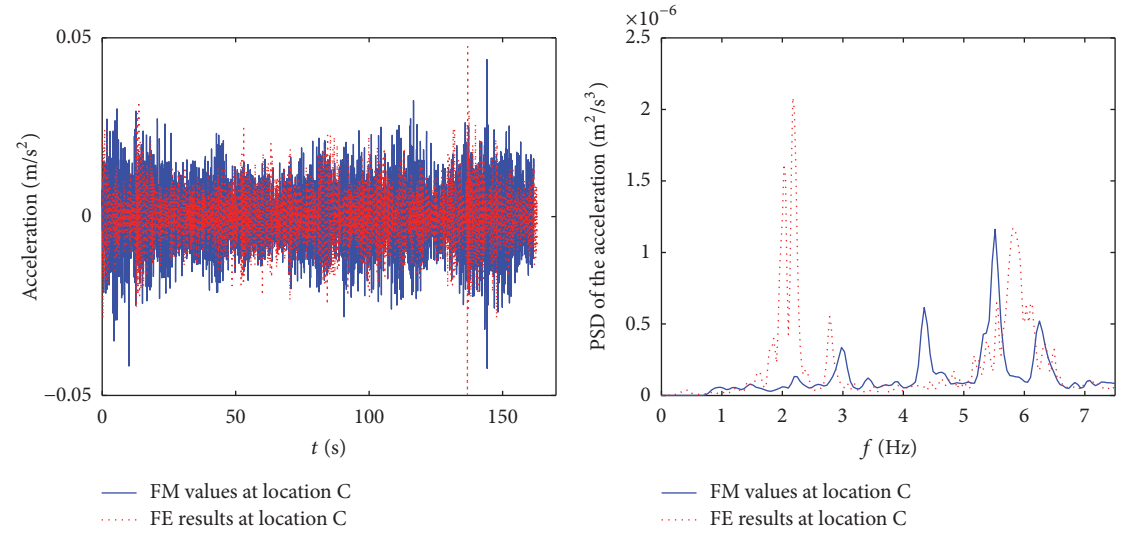

(e) Comparison of the acceleration time history at location C

(f) Comparison of the acceleration PSD at location C

Figure 9: Continued.

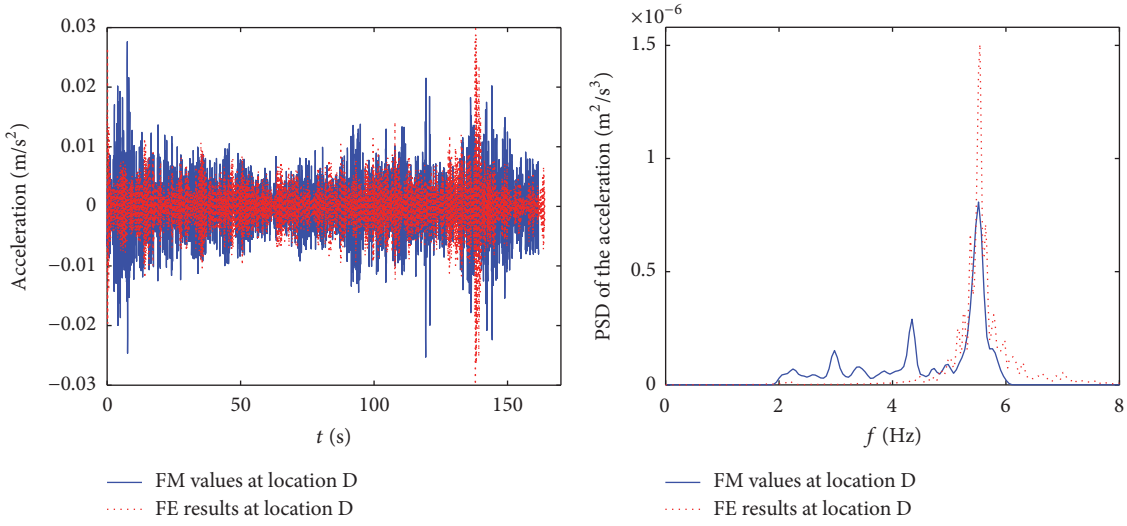

(g) Comparison of the acceleration time history at location D

(h) Comparison of the acceleration PSD at location D

Figure 9: Comparison of the results of the finite element analysis calculation and the field measurements at the different measurement locations.

Table 5: Windward area of number 160 transmission tower.

Segment numbering	Actual area (mm^2)		Projected area (mm^2)	
	Perpendicular to the transmission line direction	Parallel to the transmission line direction	Perpendicular to the transmission line direction	Parallel to the transmission line direction
(1)	865392	1528774	752023.1	1328632
(2)	1011444	5622524	410159.4	5606444
(3)	1615828	3236466	1597591	3227210
(4)	3293370	4854699	2913509	4847745
(5)	2373116	2373116	2340374	2340374
(6)	5107037	5107037	5036575	5036575
(7)	7623368	7623368	7518187	7518187
(8)	2675226	2675226	2638316	2638316

exhibits relatively large errors, which could occur because of errors in the loads input or because the responses at these locations are affected by multiple-vibration-mode in the structure and by the influence of the measurement noise.

To vividly compare the results of the finite element analysis calculation and the measured vibration characteristics in the field, the *Hilbert-Huang Transform* (HHT) method is used in this study to identify the measured dynamic response and the dynamic response calculated by the finite element analysis method. The frequency and damping results obtained are listed in Table 6. The vibration frequency in the table is the main frequency of the structural vibration caused by the wind load at these measurement locations. Because the vibration at locations B and C is the cumulative vibration of multiple vibration modes, only the results of the high-order vibration models at these two locations are given in Table 6. Table 7 presents a comparison of the maximum acceleration and the root-mean-square responses at each measurement location.

Table 6 reveals that the vibration frequencies given by the finite element calculation method in this study are in agreement with the field measurement values, but the identified damping ratios from the two methods are quite different from each other. This difference is mainly because the *Rayleigh* damping formula is used in the finite element analysis, whereas when the actual transmission tower-line system sustains wind-induced vibration, it is affected not only by the structure damping but also by the impact of pneumatic damping, thereby resulting in larger damping ratio differences between the finite element analysis and the field measurements. However, Table 7 presents that the maximum deviation of the acceleration response at these locations does not exceed 11%, and the maximum deviation of root-mean-square response does not exceed 20%, which are acceptable deviations in engineering practice. Therefore, the finite element model for the tower-line transmission system established in this study is reliable and can be used to simulate more engineering cases.

Table 6: Comparison of vibration characteristics from the finite element analysis and field measurements.

Measurement location	Vibration frequency (Hz)			Damping ratio (%)		
	Finite element calculation (a)	Field measurement (b)	Deviation ((a) − (b)/(b))	Finite element calculation (a)	Field measurement (b)	Deviation ((a) − (b)/(b))
A	1.98	1.97	0.51%	1.18	1.54	−23.4%
B	5.93	5.62	5.52%	2.61	6.28	−58.4%
C	6.47	6.22	4.02%	1.30	3.00	−56.7%
D	5.41	5.41	0.00%	1.95	2.90	−32.8%

Table 7: Comparison of the maximum acceleration and root-mean-square responses obtained from the finite element calculation and field measurements.

Measurement location	Maximum acceleration (m/s^2)			Root mean square root (m/s^2)		
	Finite element calculation (a)	Field measurement (b)	Deviation ((a) − (b)/(b))	Finite element calculation (a)	Field measurement (b)	Deviation ((a) − (b)/(b))
A	0.1091	0.1125	−3.02%	0.0250	0.0228	9.65%
B	0.1346	0.1212	11.06%	0.0197	0.0228	−13.60%
C	0.0475	0.0438	8.45%	0.007	0.008	−12.50%
D	0.0298	0.0276	7.97%	0.0038	0.0047	−19.15%

5. Comparison of the Dynamic Response of Transmission Towers in the Tower-Line System with That of a Corresponding Single Tower

Transmission tower-line systems are complex coupling systems. The coupling effect between the towers and the lines under strong wind has a great influence on the force applied on the transmission towers. However, the existing design codes for overhead transmission lines separate the design of the transmission towers and lines. The wind loads sustained by the transmission lines are applied as static loads on the hanging points of the transmission towers, whereas the wind load adjustment factor is used to approximate the effect of wind-induced vibration on the transmission lines and towers. This linear design theory is easily implemented, but it underestimates the negative effect of the tower-line coupling vibration on the transmission towers, cannot truly reflect the loading conditions of the tower-line system under strong wind loads, and may result in designs that are unsafe. To quantitatively analyze the effect of the tower-line coupled vibration on the transmission tower, this section further calculates the dynamic response of the transmission tower in the transmission tower-line system under different wind speed conditions. The results are compared with those calculated based on the quasi-static design method stipulated in the current design codes for the corresponding single tower.

5.1. Simulation of the Wind Fields in the Transmission Tower-Line System. Because the wind speed data recorded by the wind towers in the field measurements are limited, the wind speed data equivalent to the design wind speed are not recorded. Therefore, to determine the dynamic response of the transmission tower-line system under the design wind speed, to compare it with the response obtained based on the quasi-static method stipulated in the current design codes, and to understand the characteristics of wind-induced vibration in the tower-line system under different wind speeds, the wind fields of the tower-line system must be simulated.

Based on the description of the basic characteristics of winds by Simiu and Scanlan [43], we know that the wind speed at a certain height can be expressed as the sum of the average wind speed and the fluctuating wind speed. The average wind is a stable wind that does not change for a certain period of time. Its cyclic period is longer than the fundamental natural vibration period of most structures, and its loading effect on a structure can be treated as a static load. The fluctuating wind is characterized by being highly random, with a cyclic period similar to the fundamental natural vibration period of a common structure and a dynamic loading effect on the structure. The fluctuating wind is essentially that of three-dimensional turbulent winds, including the wind parallel to the blowing direction, the wind transverse to the blowing direction, and the perpendicular turbulence. However, in general, the values of the transverse wind and the turbulence are relatively small, and they can generally be ignored in high-rise structures. Therefore, in this study, the simulation of the wind fields focuses on the simulation of the wind speed time history of the fluctuating wind parallel to the blowing direction.

In accordance with China's "Load Code for the Design of Building Structures" GB50009-2012 [44], the terrain roughness of the measured transmission tower-line system is category B. The index of terrain roughness, z_0, is 0.24. According to the long-term survey data collected by the wind tower array in the field, the turbulence intensity at a height of 10 m is 10%. In this study, the modified *Davenport* spectrum is used to simulate the wind speed time history of

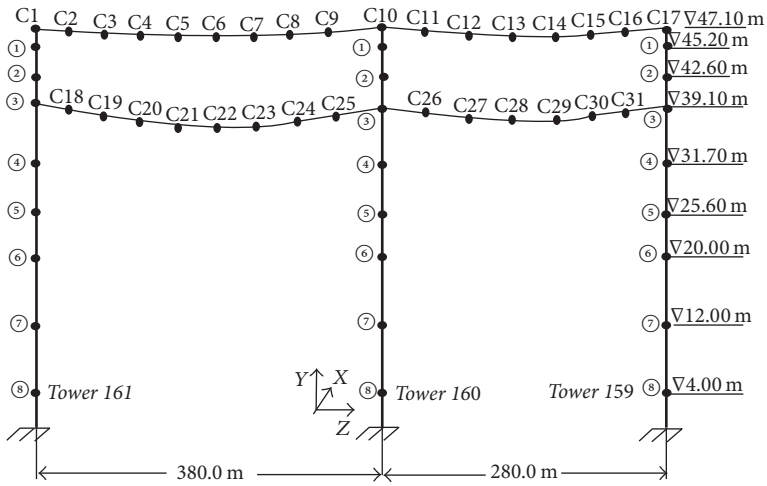

Figure 10: The representative nodal positions of the transmission tower-line system in the wind fields.

the transmission tower-line system. When simulating wind speed, the sampling frequency, f, is 10 Hz, and the simulated average wind speeds at a height of 10 m are 14, 16, 17, 18, 19, 20, 21, 22, 23, 24, and 25.3 m/s. These selected speeds include the design wind speed and, for engineering purposes, also strong wind speeds that have high probability of occurring. Therefore, these speeds can be used to analyze the characteristics of the wind-induced vibration of the tower-line system under different wind speeds. Because of the large geometric scale of the actual measured transmission lines, to simplify the workload of the calculation model, this study only simulates the wind speed for selected representative nodes of the tower-line system. The position and distribution of the representative nodes are shown in Figure 10. The direction of the fluctuating wind speed in the simulation is taken as the x-direction, that is, vertical to the transmission lines.

Wind speed is simulated at 8 nodal positions along the vertical direction of each transmission tower. Because of the large horizontal distance between the transmission towers, the correlation between the wind speeds at the adjacent transmission towers is weak, and thus only the vertical correlation is considered when simulating the wind speed time history of the transmission towers.

For the transmission lines, because the horizontal distances on either side of the tower-line system are not equal, to simulate the wind speed, the transmission lines between transmission towers number 160 and number 159 are divided into 7 sections, and the lines between transmission towers number 161 and number 160 are divided into 9 sections. The height difference between the two ends of the transmission lines is usually small, and both sides of the transmission lines satisfy the small sag assumption. Therefore, the difference in wind speeds caused by the height difference in the transmission lines can be ignored, and only the horizontal correlation of the wind speeds is considered. Additionally, the wind is regarded to be at the same speed between the two representative nodes of the transmission lines, as shown in Figure 10.

To verify the accuracy of the simulation results of the wind velocity field, the wind speeds at heights of 10 and 20 m on transmission tower number 160 are also simulated and compared with the field measurements, as shown in Figure 11. The simulated average field wind speeds at heights of 10 and 20 m are 6.03 and 7.15 m/s, respectively. It can be observed that the simulated results are generally in good agreement with the measurement results.

Based on the conditions discussed above, when the design wind speed, $U_{10} = 25.3$ m/s (i.e., the average wind speed at 10 m in height is 25.3 m/s), is set as the target wind speed, the wind speed time history at certain representative nodes in the tower-line system is shown in Figures 12 and 13. Figure 14 shows the wind speed power spectrum density at some representative nodes simulated in this study, when the design wind speed is set as the target. The energy dissipation region of the wind fields in this transmission line section is in the 0–0.2 Hz frequency band.

5.2. Wind-Induced Vibration Response of the Transmission Tower in the Tower-Line System under Two Different Wind Speeds. After the calculations of the wind speed time history, it can be converted into the wind loads on the tower-line system based on the method discussed in Section 4.2. The direction that the wind loads are applied is assumed to be perpendicular to the transmission lines (the x-direction); that is, the wind angle is 90 degrees. In such circumstances, the windward members of the transmission tower mainly sustain tensile stress, whereas the leeward side members mainly sustain compressive stress.

By using the implicit *Newmark-β* stepwise integration method, a transient dynamic time history analysis can be performed. Because the design wind load is so large that it might result in inelastic response of the angle members, the material nonlinearity of the angle members and the geometric nonlinearity of the transmission lines are accounted for simultaneously in the analysis. To more accurately determine the high-order response of the structure, the integration time

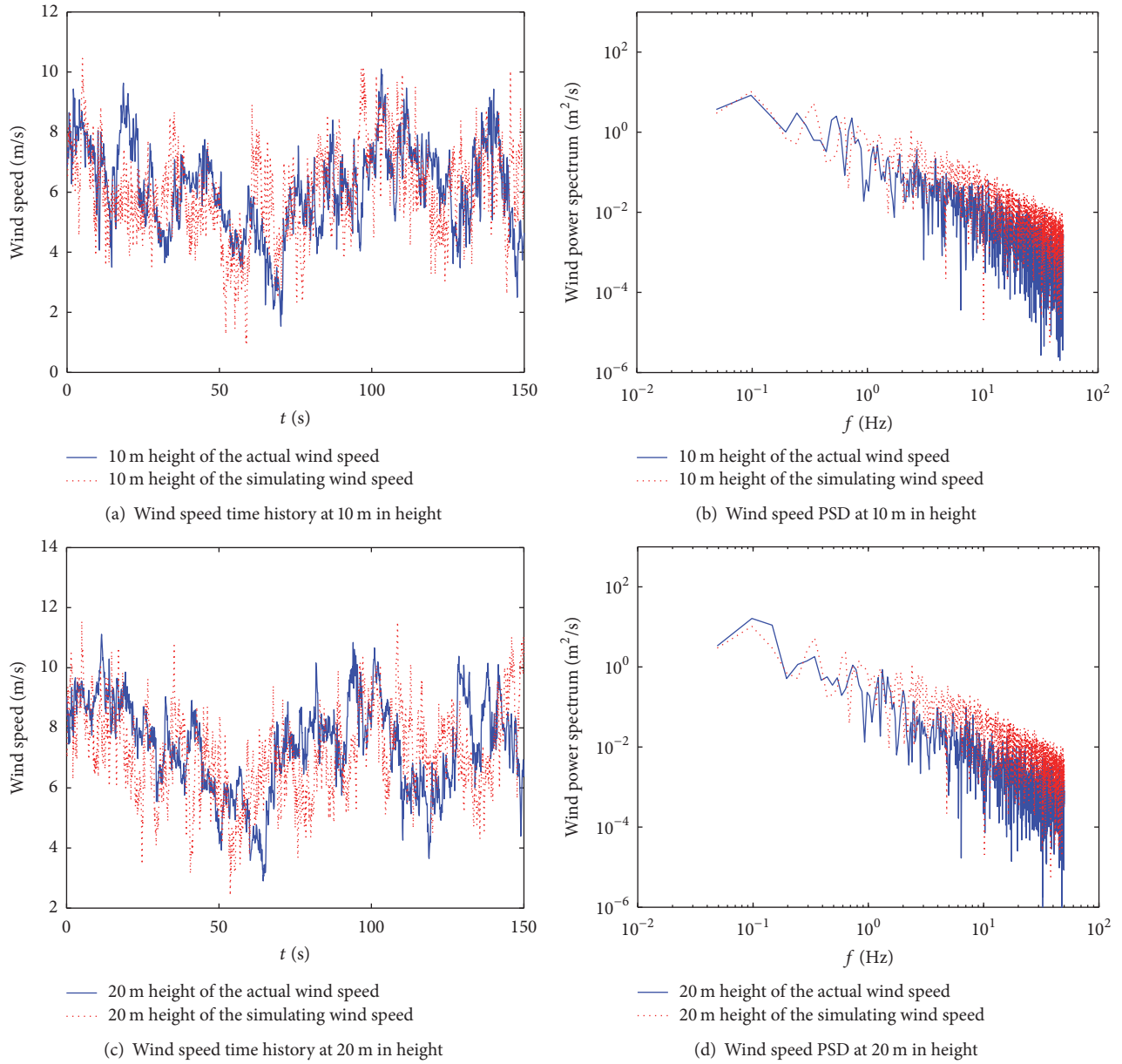

(a) Wind speed time history at 10 m in height

(b) Wind speed PSD at 10 m in height

(c) Wind speed time history at 20 m in height

(d) Wind speed PSD at 20 m in height

FIGURE 11: Comparison of the simulated results and the field measurements of wind velocity at heights of 10 and 20 m on transmission tower number 160.

step is set to 0.0025 s. For the input load with a sampling frequency of 10 Hz and a collection period of 150 s, a total of 60,000 load substeps are calculated.

To better understand the calculation results of the wind-induced vibration response of the tower in the tower-line system and to compare them with the calculation results of the corresponding single tower under different wind speeds, in this section, the measuring positions on transmission tower number 160 in the tower-line system are described. As shown in Figure 15, the letter "N" indicates the node, "E" represents the element, the number after the letter is the sequence number of the node or element, and the letters in brackets correspond to the placement locations of the acceleration sensors on tower number 160 (see Figure 5).

5.2.1. Responses of the Transmission Tower under the Low Wind Speed (U_{10} = 6.03 m/s). The presented work is mainly focused on the displacement and acceleration responses on the top of the tower and on the maximum stress of the tower members.

(1) The Displacement and Acceleration Responses of the Nodes at the Top of the Tower. The node displacement and acceleration time history responses and the corresponding PSD at the top of transmission tower number 160 under a wind speed of U_{10} = 6.03 m/s at two different nodes on the top of the tower are shown in Figures 16 and 17.

It can be observed from the figures shown above that the displacement at the top of the tower in the tower-line system is much greater than that for the corresponding single tower.

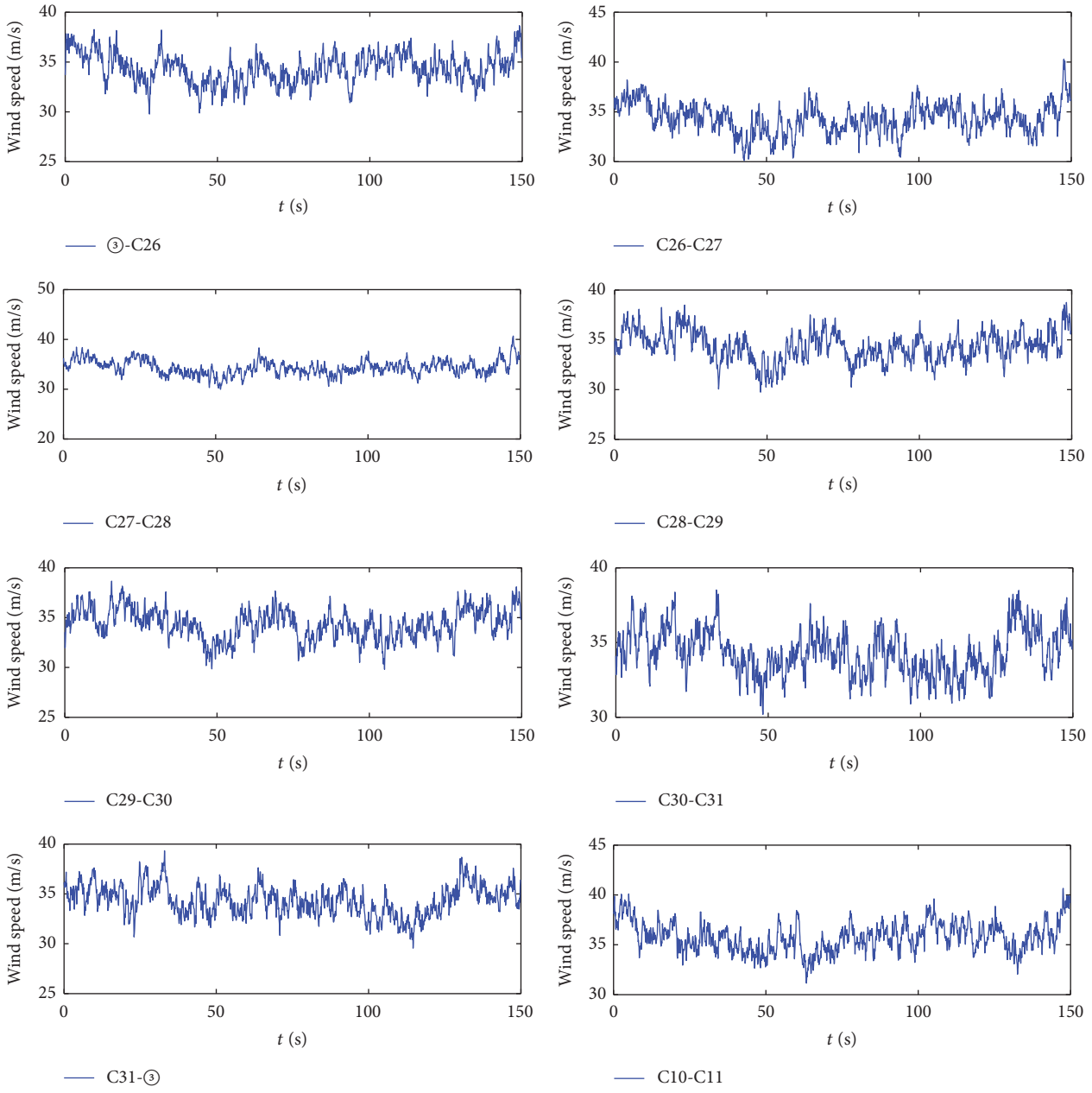

Figure 12: The simulated wind speed time history of the transmission lines between transmission towers number 159 and number 160.

The x-direction acceleration time history curves indicate that there is no obvious difference between the tower in the tower-line system and the corresponding single tower under the low wind speed (U_{10} = 6.03 m/s), whereas the z-direction results differ greatly between the two. From the frequency spectrum diagrams, we can also see that the tower vibration energy in the x-direction is mainly distributed in the frequency band of 1.8–2.2 Hz, which is very close to the fundamental natural frequency of the corresponding single tower in the x-direction. However, in the z-direction, there is a large difference, indicating that the vibration of the transmission tower is more complicated in the tower-line system than in the single tower.

(2) Stress Responses of the Tower Members. The stress time history and the PSD at several different elements of the tower in the tower-line system wind speed of U_{10} = 6.03 m/s are shown in Figures 18 and 19, respectively.

Figure 18 shows that, under the low wind speed (U_{10} = 6.03 m/s), the maximum stress of multiple members of the tower in the tower-line system is much less than the material design yield strength. Figure 19 shows that the maximum tensile stress (or compressive stress) of the main members of the tower in the tower-line system is caused by multimode vibration. The vibration energy is mainly distributed in the frequency band of 0–0.5 Hz, which is far from the fundamental natural frequency of the corresponding single tower.

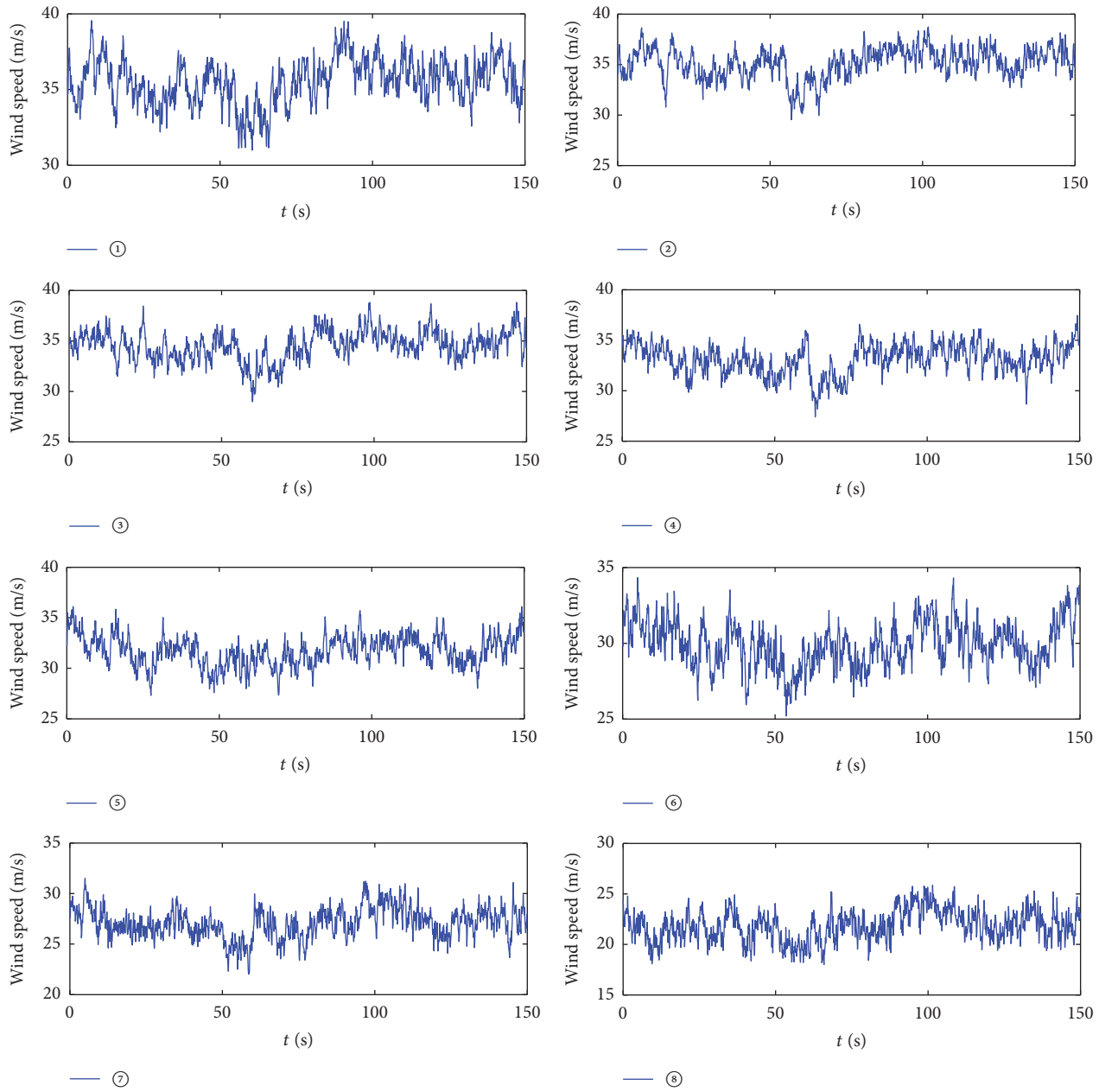

Figure 13: The simulated wind speed time history at the representative nodes on transmission tower number 160.

The frequency of the peak value of each high-order vibration model has an approximately multiplying relationship with the frequency of the peak value of its 1st model. Even the frequencies of the peaks of some high models also have an approximately multiplying relation.

5.2.2. Responses of the Transmission Tower under the Design Wind Speed, U_{10} = 25.3 m/s

(1) The Displacement and Acceleration Responses of the Nodes at the Top of the Tower. The node displacement and acceleration time history responses and the corresponding PSD at the top of transmission tower number 160 under the design speed wind (U_{10} = 25.3 m/s) at two different nodes at the top of the tower are shown in Figures 20 and 21.

To demonstrate the influence of wind-induced vibration on the transmission tower in the tower-line system, the dynamic steady-state response of the corresponding single tower under the design wind speed (U_{10} = 25.3 m/s) is also calculated. Comparisons of the displacement and acceleration responses at the corresponding nodes are presented in Tables 8 and 9, respectively.

Table 8 reveals that, under the design wind speed (U_{10} = 25.3 m/s), the displacement at the top of the tower in the tower-line system is much greater than that for the corresponding single tower. The maximum displacement in the x-direction for the tower-line system is approximately 5.2

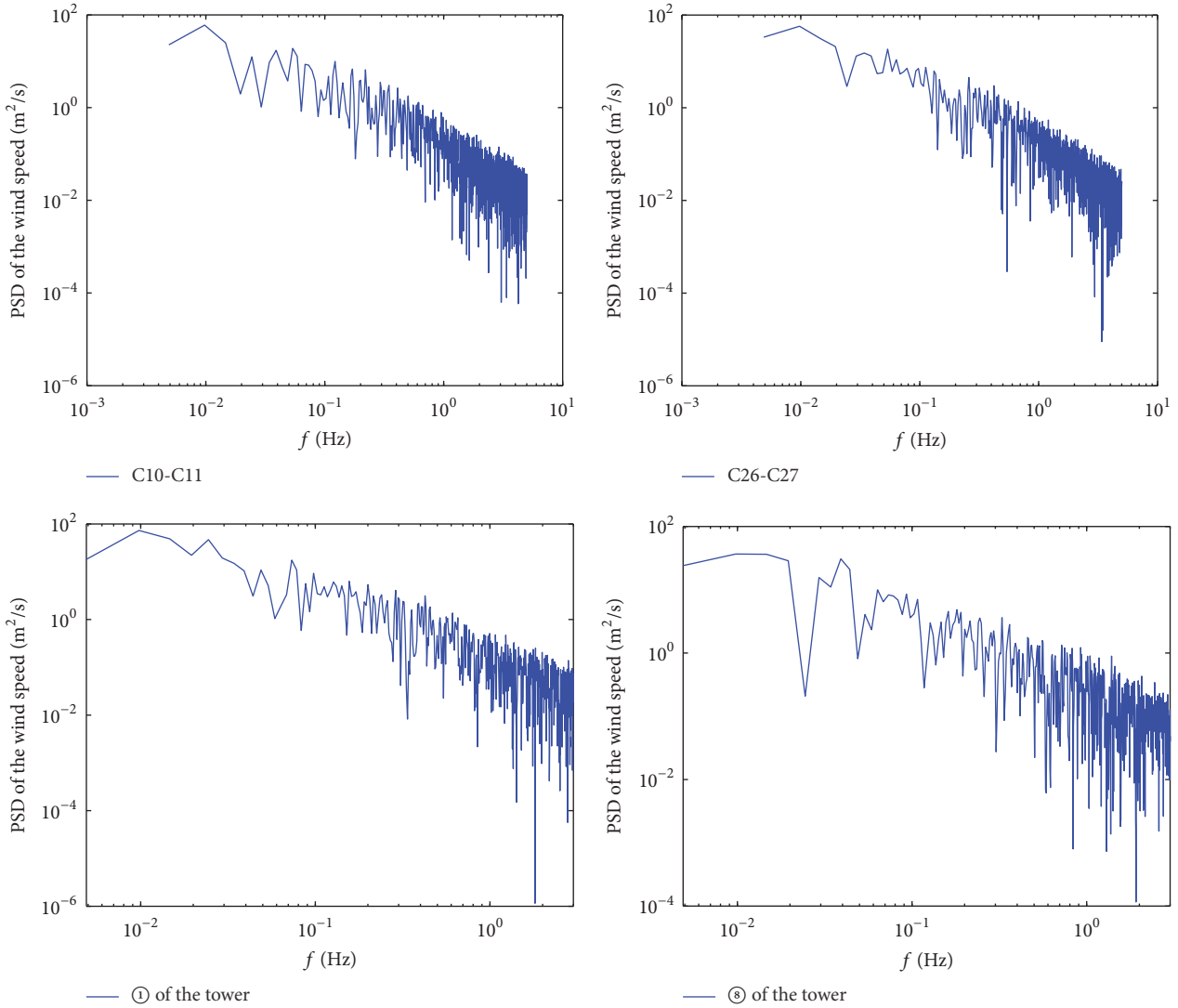

Figure 14: The simulated wind speed PSD on certain representative nodes on the transmission tower-line system.

Table 8: Comparison of the dynamic analysis results of the displacement at the top of the transmission tower for the single tower and the tower-line system under a wind speed of U_{10} = 25.3 m/s.

Node number	Maximum value			Average			Root mean square		
	TL	ST	TL/ST	TL	ST	TL/ST	TL	ST	TL/ST
	x-direction displacement at the top of the tower (m)								
727	0.26	0.05	5.2	0.20	0.03	6.7	0.01	0.004	2.5
660	0.20	0.04	5.0	0.16	0.03	5.3	0.01	0.003	3.3
	z-direction displacement at the top of the tower (m)								
727	0.07	0.0008	87.5	0.02	0.0004	50	0.02	0.0001	200
660	0.04	0.0008	50	0.01	0.0005	20	0.01	0.0001	100

Note. In the table, TL represents the response value of the tower in the tower-line system, and ST represents the response value of the corresponding single tower.

times that for the single tower. The displacement in the z-direction at the top of the tower can be as great as 7 cm, whereas in the corresponding single tower, this value is close to 0. The results presented in Table 9 demonstrate that the maximum acceleration and root-mean-square values in the x-direction at the top of the tower in the tower-line system are less than the response values of the corresponding single tower, whereas the time history curves in Figures 20 and 21 reveal no obvious difference between the two. In addition, the maximum acceleration in the z-direction at the top of the

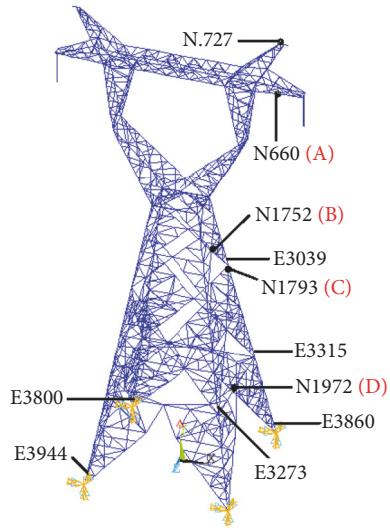

Figure 15: Measuring locations of the nodes and elements on transmission tower number 160.

Table 9: Comparison of the dynamic analysis results of the acceleration at the top of the transmission tower for the single tower and the tower-line system under a wind speed of U_{10} = 25.3 m/s.

Node number	Maximum value			Root mean square		
	TL	ST	TL/ST	TL	ST	TL/ST
x-direction acceleration at tower top (m/s^2)						
727	1.10	1.98	0.56	0.34	0.50	0.68
660	0.87	1.56	0.56	0.26	0.39	0.67
z-direction acceleration at tower top (m/s^2)						
727	0.59	0.10	5.9	0.13	0.03	4.3
660	0.45	0.08	5.63	0.09	0.03	3.0

Note. In the table, TL represents the response value of the tower in the tower-line system, and ST represents the response value of the corresponding single tower.

tower in the tower-line system is 5.9 times that in the corresponding single tower, and the root-mean-square response value is 4.3 times that in the single tower.

Similar to the results described in the previous section, we can also find that, from the frequency spectrum diagrams in Figures 20 and 21, the main frequency band of the tower vibration energy in the x-direction is narrow and the peak value is close to the fundamental natural frequency of the corresponding single tower in the x-direction, whereas the one in the z-direction is distributed in a wide range, with obvious peak values in the lower frequency range.

(2) Stress Responses of the Tower Members. The stress time history and the PSD at several different elements of the tower in the tower-line system under the design wind speed (U_{10} = 25.3 m/s) are shown in Figures 22 and 23, respectively.

Figure 22 shows that, under the design wind speed (U_{10} = 25.3 m/s), the maximum compressive stress of multiple members of the tower in the tower-line system can reach 310 MPa, close to the material design yield strength. Figure 23 demonstrates that the maximum stress of the main members of the tower in the tower-line system is caused by multimode vibration. The vibration energy is mainly distributed in the frequency band of 0-1 Hz, which is also far from the fundamental natural frequency of the corresponding single tower. Similarly, the frequency of the peak value of each high-order vibration model has an approximately multiplying relationship with the frequency of the peak value of its 1st-model.

To further understand the influence of the vibration of the transmission lines on the main members of the tower in the tower-line system, the steady-state time history response of the main members in the corresponding single tower under the design wind speed (U_{10} = 25.3 m/s) is calculated in this section. When calculating the dynamic response of the corresponding single tower, the wind loads are applied along the height of the tower, as shown in Figure 8. At the same time, the deadweights of the conductors, the ground wires, the insulators, and the fittings are applied on the hanging points of the tower. In addition, the wind loads sustained by the transmission lines under the design wind speed should also be applied on the hanging points of the tower simultaneously. The stress PSD of the main members of the corresponding single tower is also calculated (Figure 24).

Figure 24 shows that the peak frequencies corresponding to the stress PSD of elements number 3800 and 3944 in the single tower are 0.05 and 2.07 Hz, respectively. The vibration energy is mainly concentrated in the mode corresponding to 2.07 Hz, which is very close to the free vibration mode frequency of 2.1481 Hz, caused by the single tower bending along the x-direction, indicating that the stress increase in the members of the single tower is mainly caused by the wind load and the vibration of the tower itself.

Comparing Figures 23 and 24, the stress PSD of the tower in the tower-line system is mainly distributed in the range of 0–0.5 Hz, and the frequency corresponding to the peak of the PSD is close to the 1st–4th low-order natural frequencies of the tower-line system and far from the natural frequency of the single tower (see Table 4), thus indicating that the stress increase in the transmission tower in the tower-line system is mainly caused by the vibration of the transmission lines.

Table 10 presents a comparison of the dynamic stress of the tower in the tower-line system and the corresponding single tower under the design wind speed (U_{10} = 25.3 m/s). The results summarized in Table 10 demonstrate that, under the same design wind speed, the maximum stress of multiple members in the tower-line system can reach the design yield strength of the steel. The stress values in the tower-line system are much greater than those of the corresponding single tower. Therefore, under the design wind speed, the transmission tower in the tower-line system could be destroyed, but the corresponding single tower remains safe, demonstrating that the amplifying effect of the dynamic coupling between the transmission line and the transmission tower in the tower-line system on the dynamic response of the transmission tower cannot be neglected.

In general, the coupling effect between the transmission lines and the transmission tower is the intrinsic property of the tower-line system. Because of the coupling effect in the

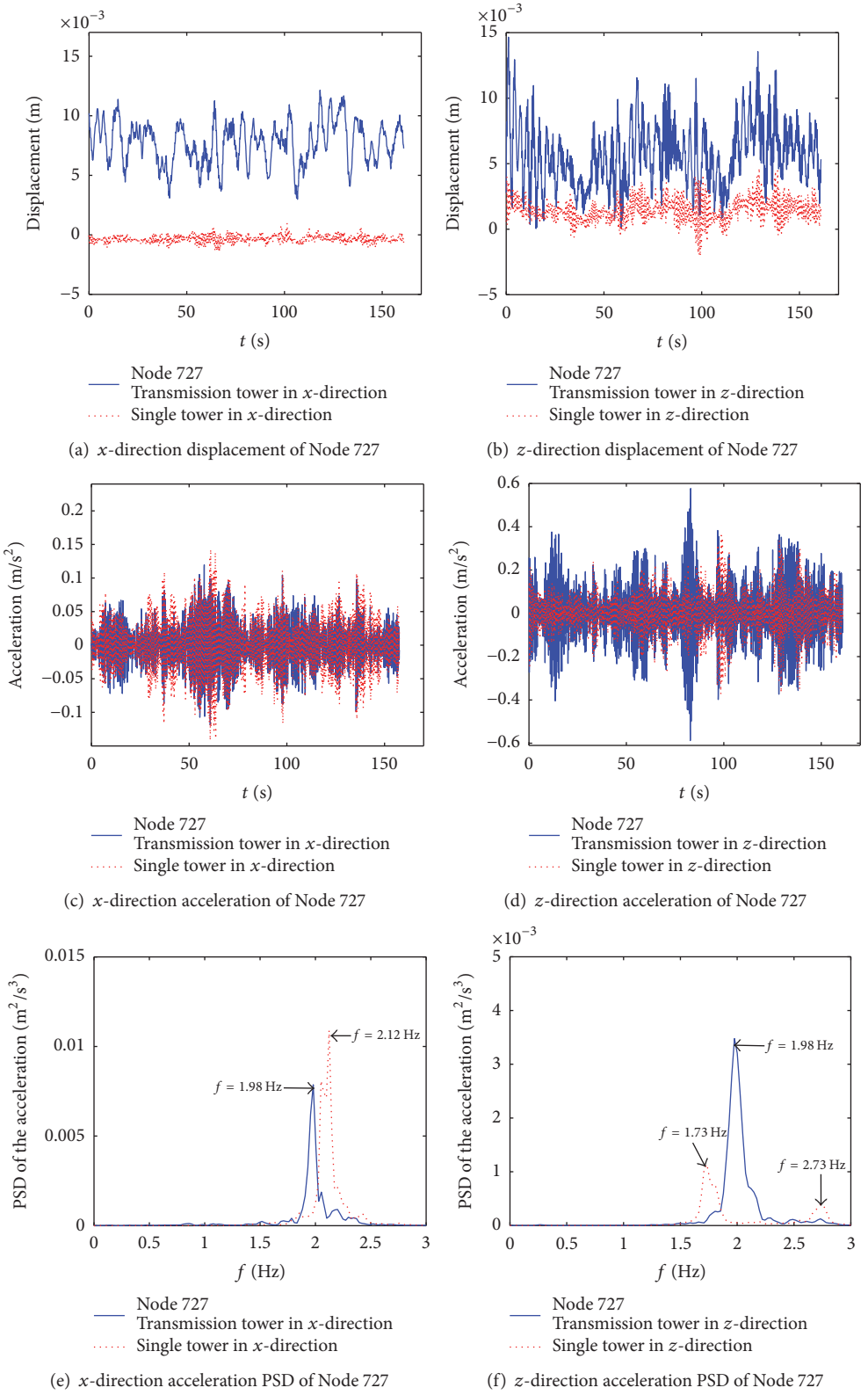

FIGURE 16: Steady-state response of Node 727 of the tower under a wind speed of U_{10} = 6.03 m/s.

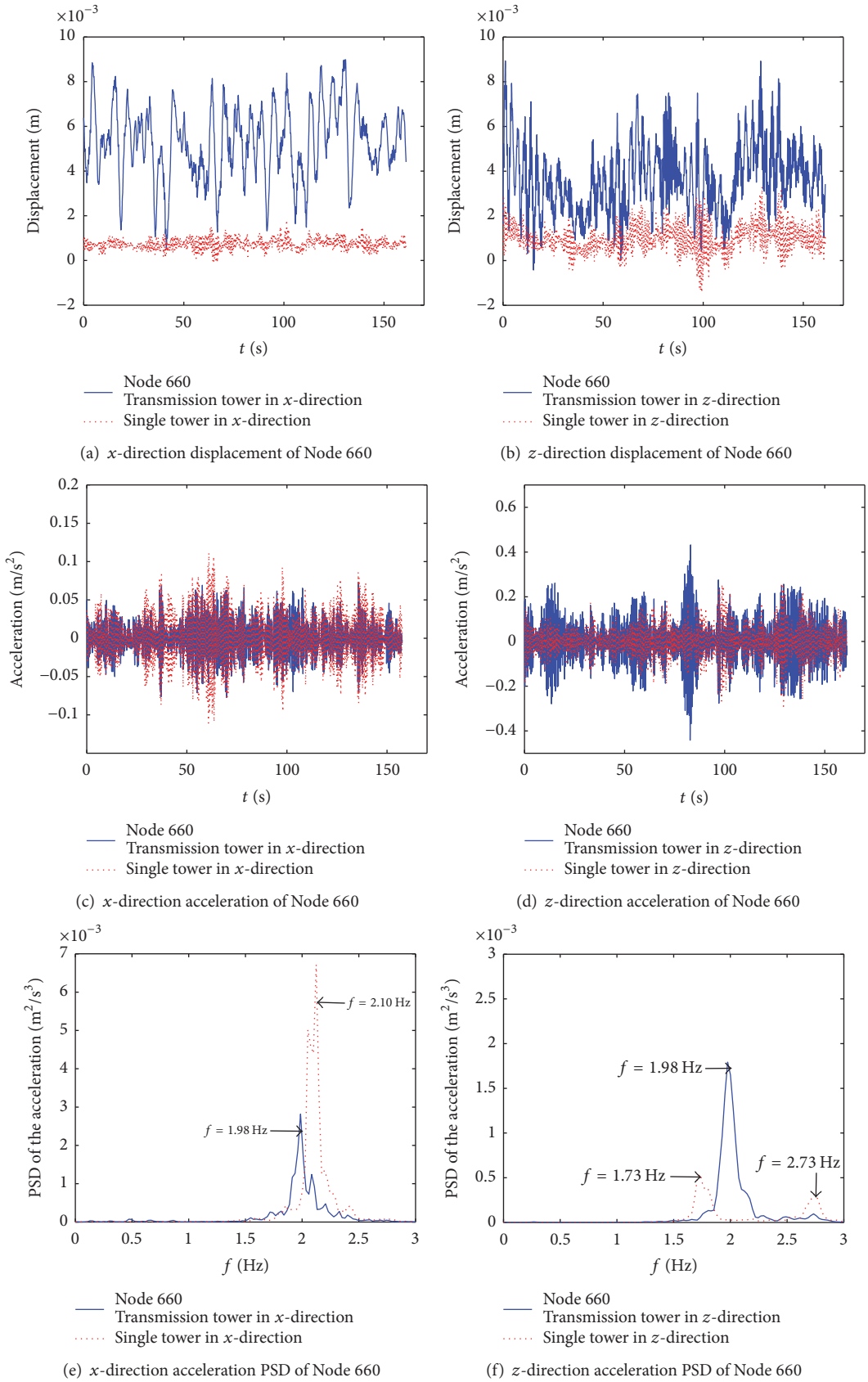

(a) x-direction displacement of Node 660

(b) z-direction displacement of Node 660

(c) x-direction acceleration of Node 660

(d) z-direction acceleration of Node 660

(e) x-direction acceleration PSD of Node 660

(f) z-direction acceleration PSD of Node 660

FIGURE 17: Steady-state response of Node 660 of the tower under a wind speed of U_{10} = 6.03 m/s.

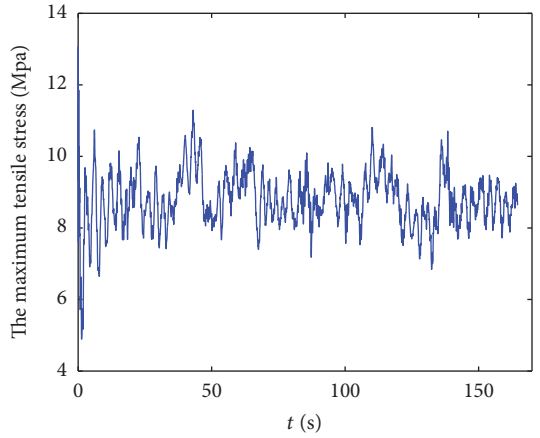

(a) Maximum tensile stress time history for element number 3800

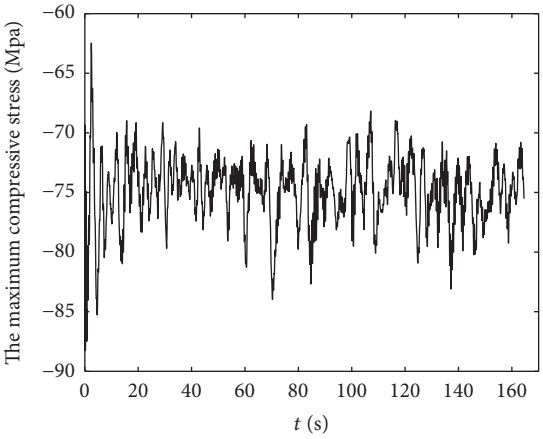

(b) Maximum compressive stress time history for element number 3944

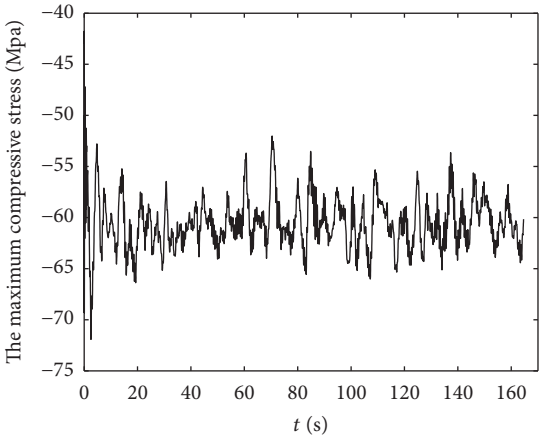

(c) Maximum compressive stress time history for element number 3039

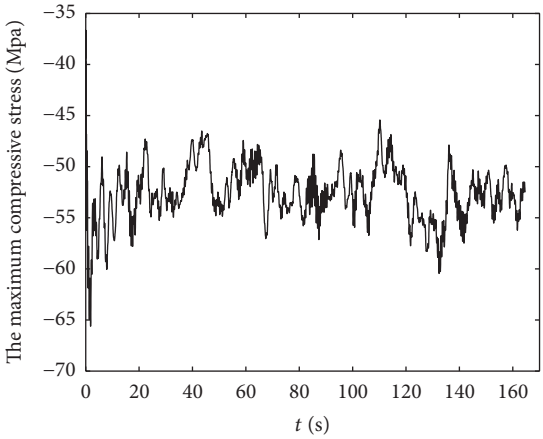

(d) Maximum compressive stress time history for element number 3273

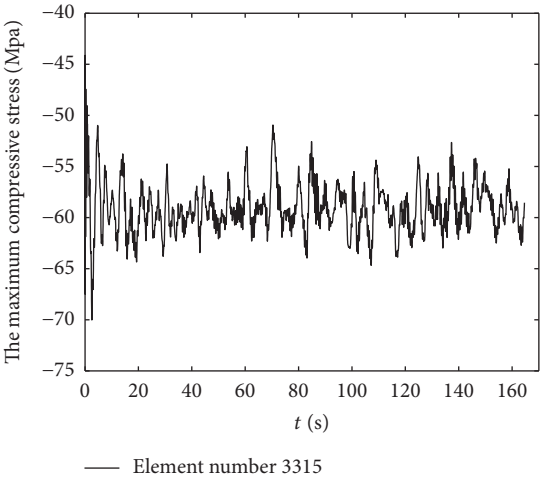

(e) Maximum compressive stress time history for element number 3315

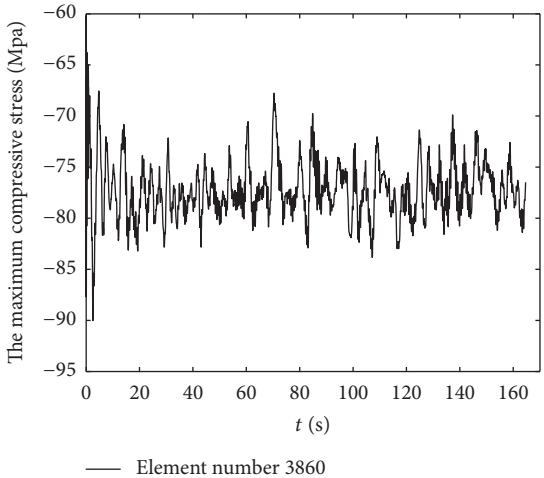

(f) Maximum compressive stress time history for element number 3860

FIGURE 18: Stress time history of the main members of the transmission tower in the tower-line system under a wind speed of U_{10} = 6.03 m/s.

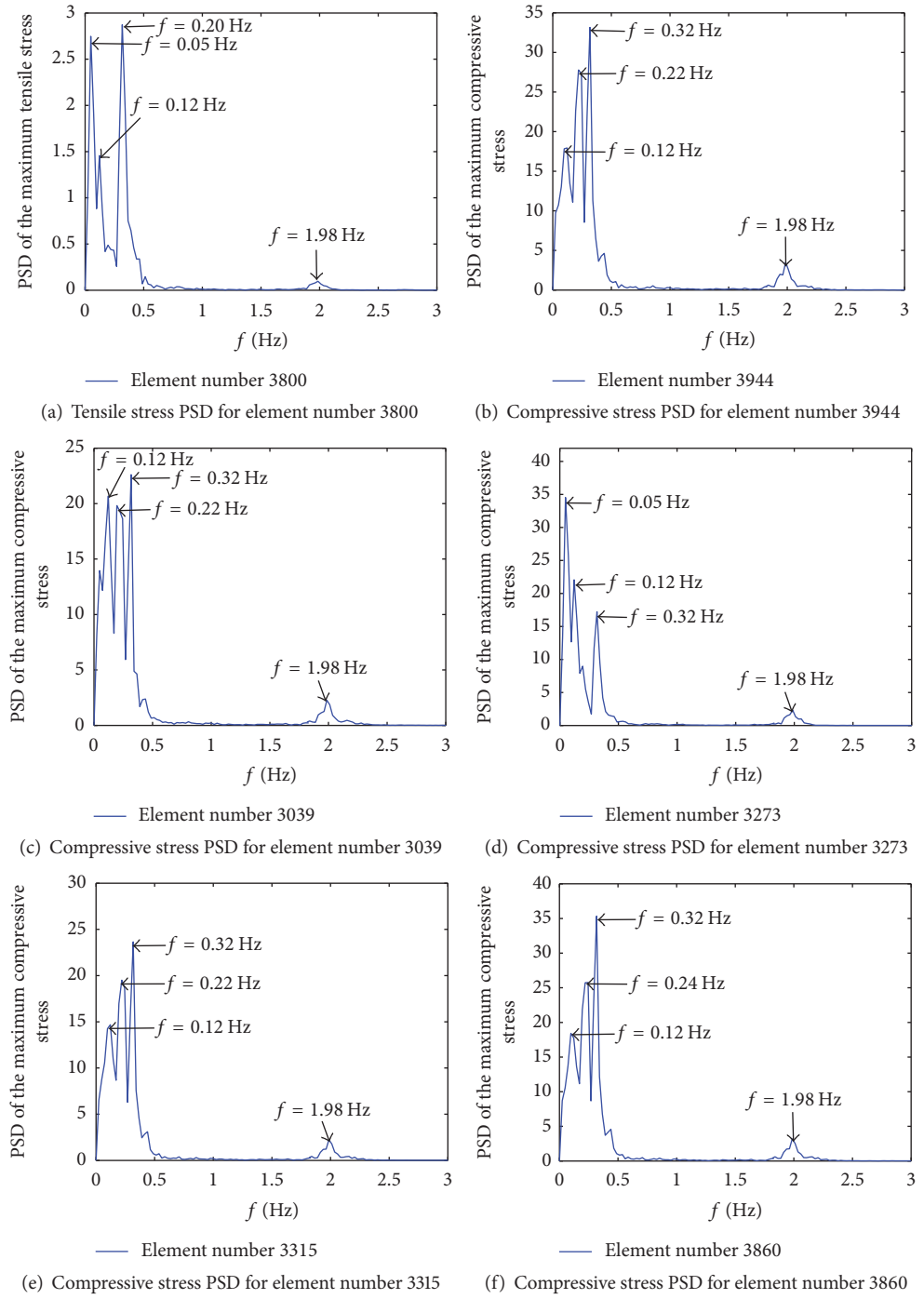

Figure 19: The stress PSD of the main members of the transmission tower in the tower-line system under a wind speed of U_{10} = 6.03 m/s.

tower-line system, the vibration of the transmission tower is more complicated and stronger in the tower-line system than in the single tower; that is, the coupling effect between the tower and the lines amplifies the vibration effect on the transmission tower. Comparing the frequency spectrum results in Figures 16, 17, 20, and 21, the coupling effect is less obvious under the low wind speed (i.e., U_{10} = 6.03 m/s) than that under the strong wind speed (i.e., U_{10} = 25.3 m/s). Although the results shown in Figure 19 demonstrate that the maximum stress of multiple members of the tower in the tower-line system contains significant coupling vibration contributions, the coupling effect is too often neglected due to the small absolute value of the stress. However, under the strong wind speed (i.e., U_{10} = 25.3 m/s), the coupling effect on the responses of the tower becomes very prominent, resulting in the potential premature failure of the tower-line system, which indicates that wind speed plays an important role in the tower-line coupling effect.

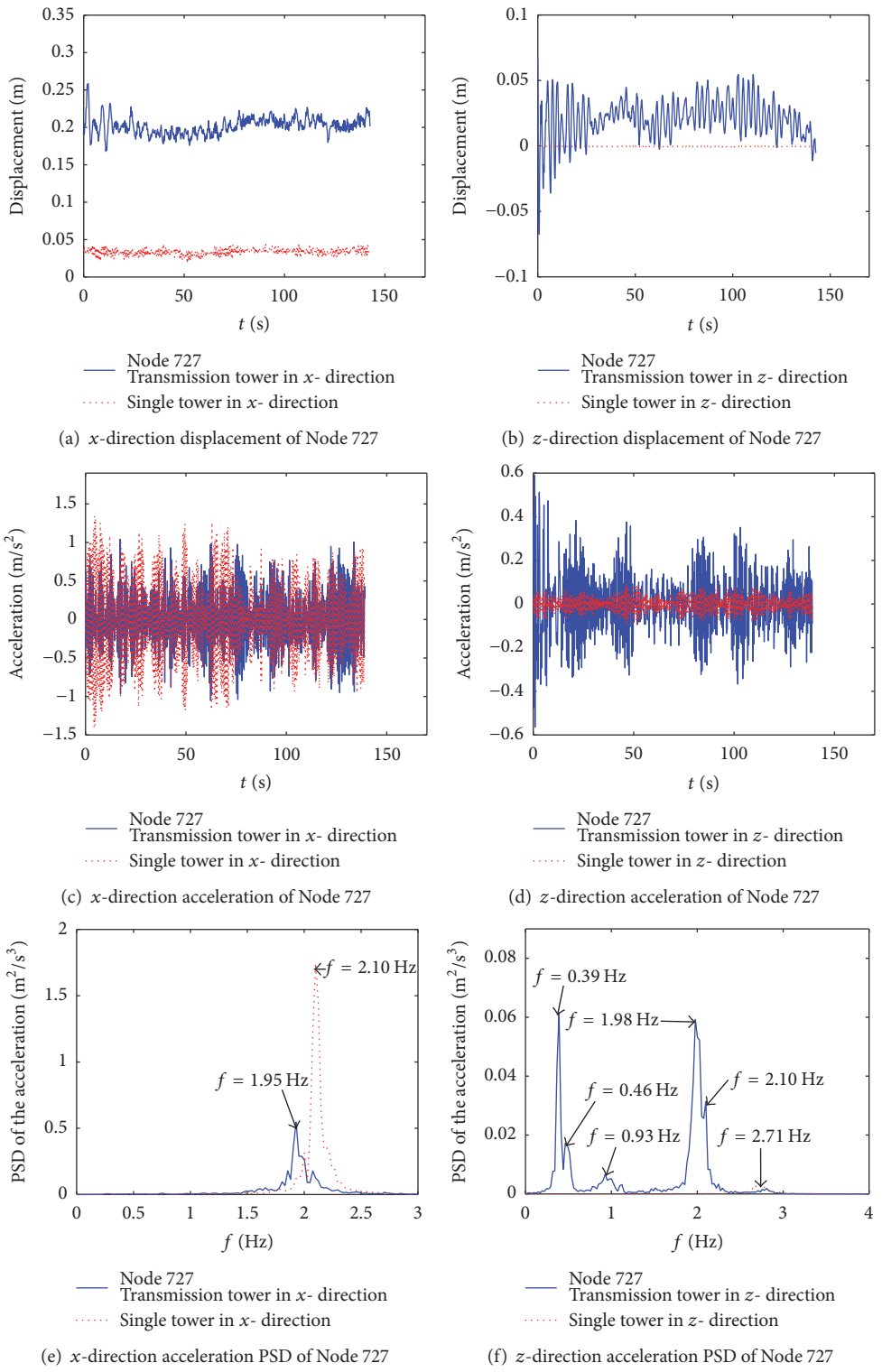

FIGURE 20: Steady-state response of Node 727 of the tower under the design wind speed (U_{10} = 25.3 m/s).

5.3. The Comparative Analysis of the Wind-Induced Vibration Response of the Transmission Tower in the Tower-Line System and the Quasi-Static Response of the Corresponding Single Tower. At present, in the structural design of transmission tower-line systems, the transmission tower is usually separated from the transmission lines. In the design of a transmission tower, the quasi-static method is used. In this method, the wind loads sustained by the transmission lines are applied to the transmission tower as the external concentration force. The influence of the wind-induced vibration

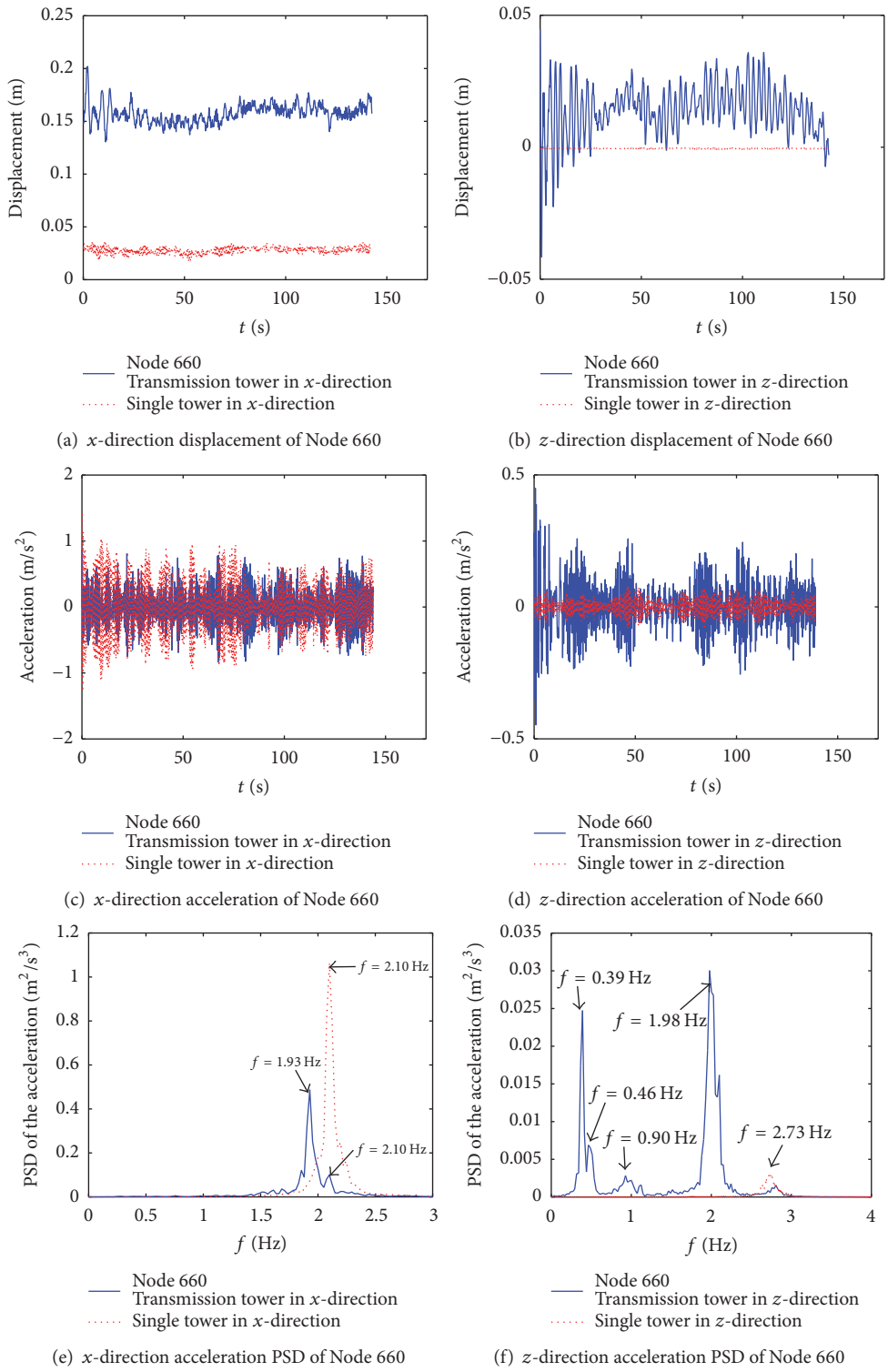

FIGURE 21: Steady-state response of Node 660 of the tower under the design wind speed (U_{10} = 25.3 m/s).

of the transmission lines on the dynamic characteristics of the transmission tower is disregarded. To quantitatively analyze the influence of the coupled vibration in the tower-line system on the structural design of the transmission tower, based on the design method stipulated in China's "Technical Codes for Designing 110 kV–750 kV Overhead Transmission Lines" (GB50545-2010) [39], in this section, the wind loads of different strong wind speeds on the transmission lines are

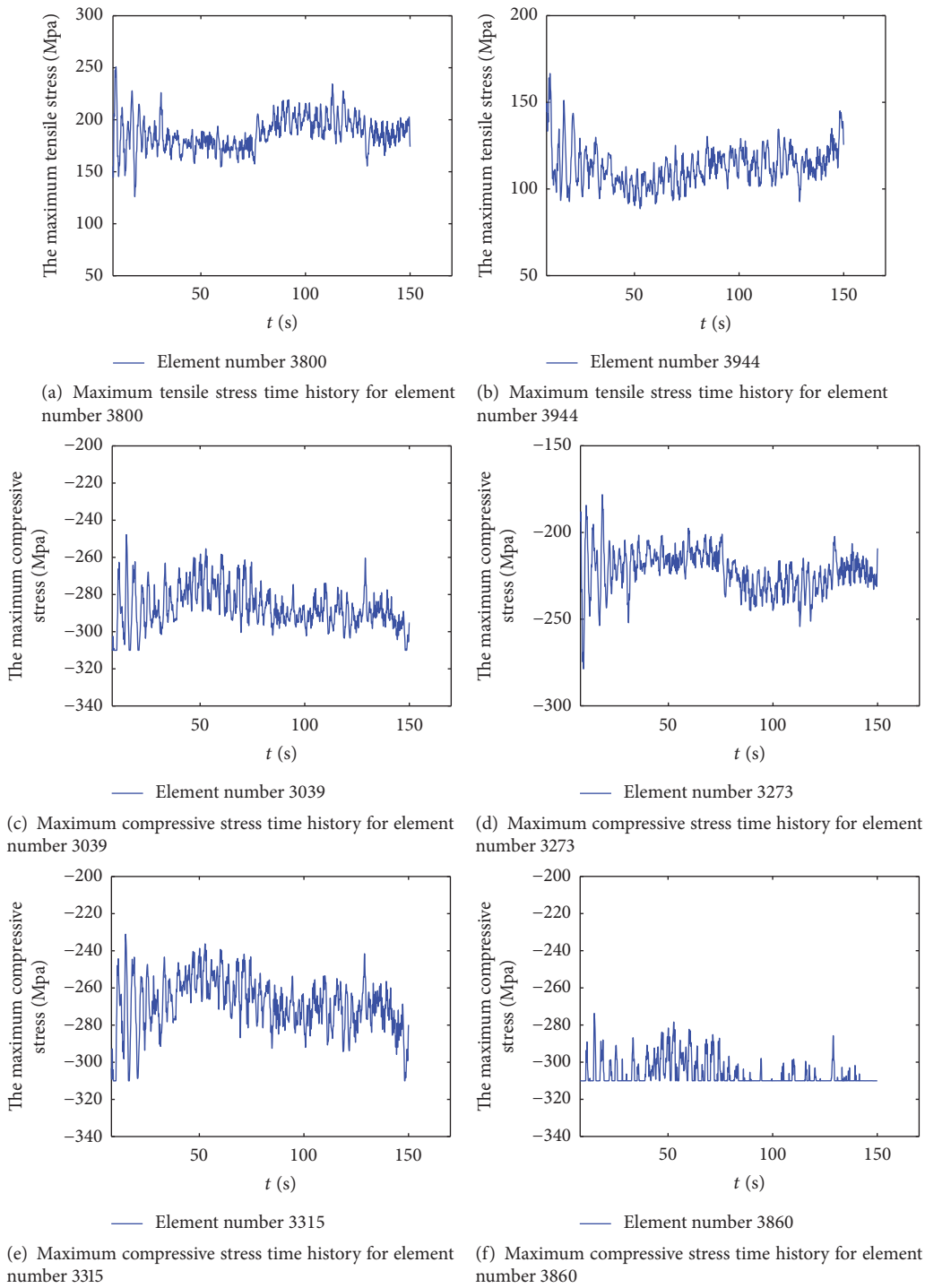

(a) Maximum tensile stress time history for element number 3800

(b) Maximum tensile stress time history for element number 3944

(c) Maximum compressive stress time history for element number 3039

(d) Maximum compressive stress time history for element number 3273

(e) Maximum compressive stress time history for element number 3315

(f) Maximum compressive stress time history for element number 3860

FIGURE 22: Stress time history response of the main members of the transmission tower in the tower-line system under the design wind speed (U_{10} = 25.3 m/s).

applied on the hanging locations of the transmission tower as external forces. The wind loads on the transmission tower are again divided into 8 segments, as shown in Figure 10.

The different wind speed conditions in the comparison include the following: average wind speeds at 10 m in height of 14, 16, 17, 18, 19, 20, 21, 22, 23, 24, and 25.3 m/s; to facilitate the identification of wind speed in the following analysis, the following symbols are used: U_{10} = 14 m/s, U_{10} = 16 m/s, U_{10} = 17 m/s, U_{10} = 18 m/s, U_{10} = 19 m/s, U_{10} = 20 m/s, U_{10} = 21 m/s, U_{10} = 22 m/s, U_{10} = 23 m/s, U_{10} = 24 m/s, and U_{10} = 25.3 m/s, respectively.

In the actual environment, the directions of the wind loads are more complex, and various angles between the wind and transmission lines exist. Therefore, to understand the

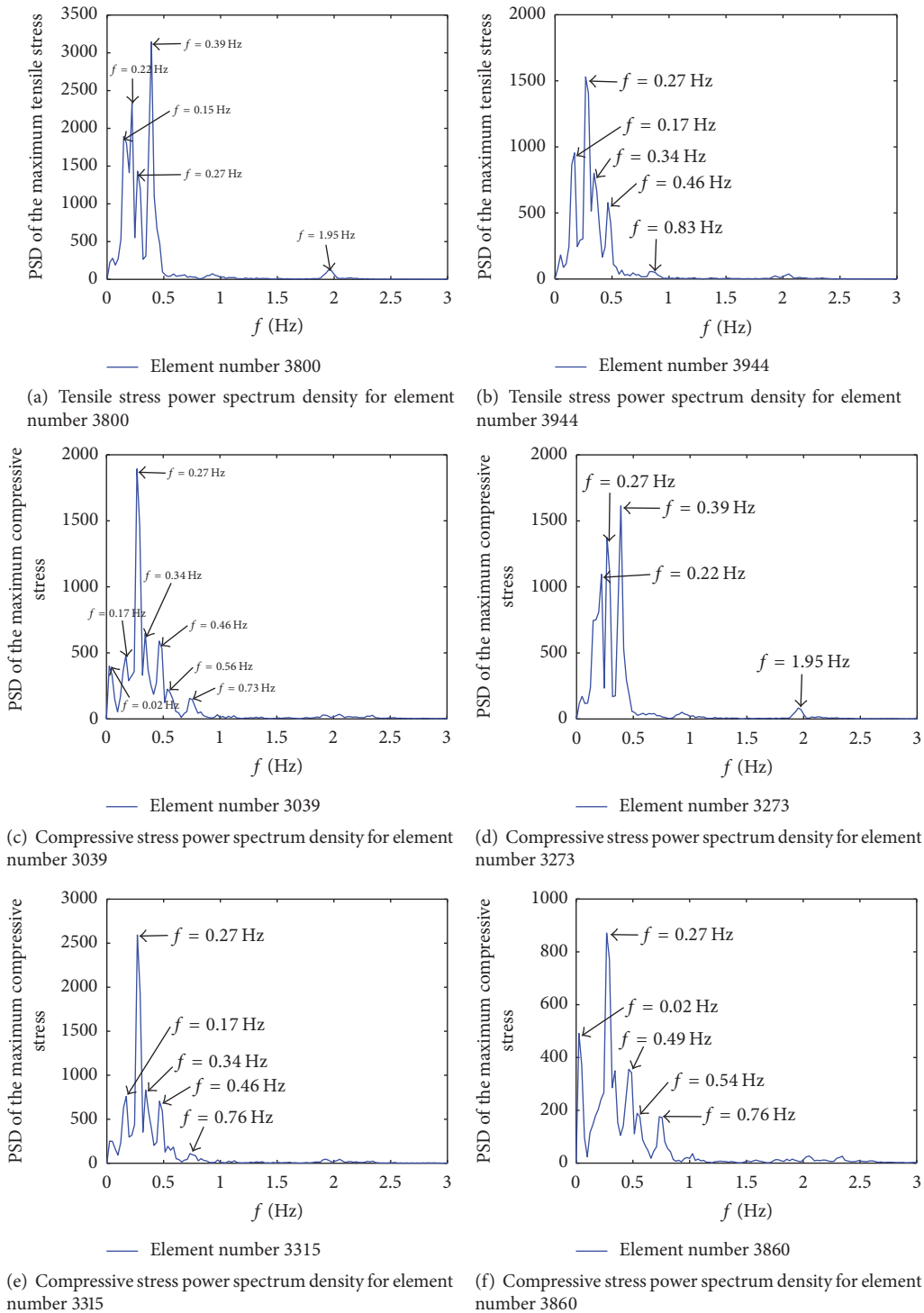

(a) Tensile stress power spectrum density for element number 3800

(b) Tensile stress power spectrum density for element number 3944

(c) Compressive stress power spectrum density for element number 3039

(d) Compressive stress power spectrum density for element number 3273

(e) Compressive stress power spectrum density for element number 3315

(f) Compressive stress power spectrum density for element number 3860

FIGURE 23: The stress PSD of the main members of the transmission tower in the tower-line system under the design wind speed (U_{10} = 25.3 m/s).

extent of the influence of the complexity of wind directions, in this section, the wind loads applied perpendicularly to the transmission line (i.e., wind angle of 90 degrees) is first calculated and analyzed, and the results are directly compared to the dynamic calculation results of the tower-line system discussed previously. Then, wind direction angles of 60, 45, and 0 degrees (i.e., parallel to the transmission line direction) are analyzed and compared.

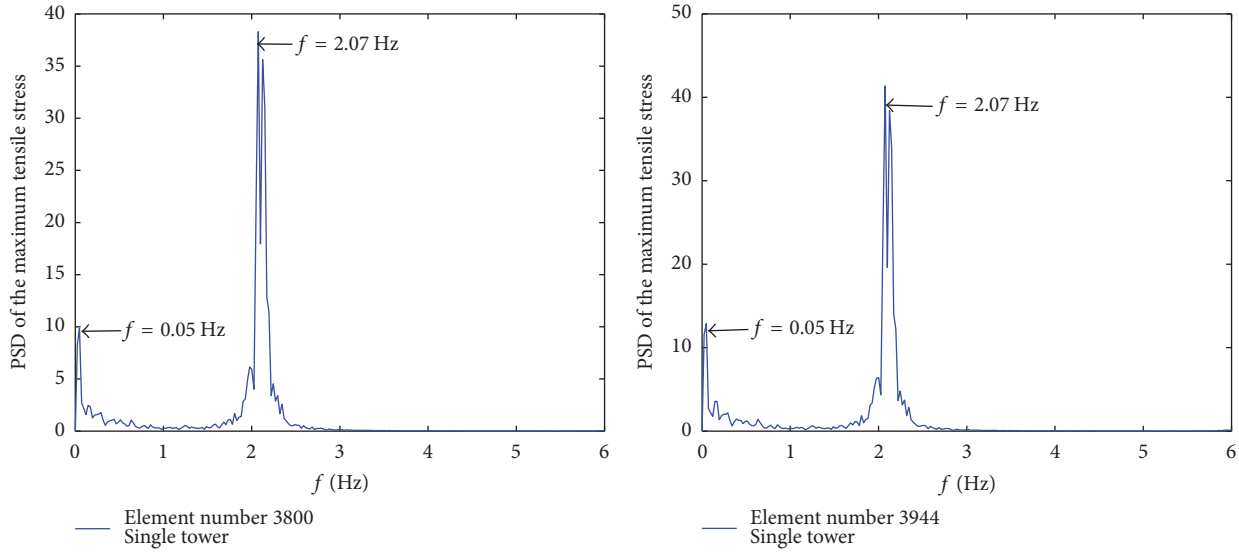

(a) Tensile stress power spectrum density in element number 3800

(b) Tensile stress power spectrum density in element number 3944

Figure 24: Stress PSD of the main members of the corresponding single transmission tower under the design wind speed (U_{10} = 25.3 m/s).

Table 10: Comparison of the dynamic stress results of the main members of the transmission tower in the tower-line system with the corresponding single tower under a wind speed of U_{10} = 25.3 m/s.

Element number	Stress of transmission tower members (MPa)								
	Maximum value			Average			Root mean square		
	TL	ST	TL/ST	TL	ST	TL/ST	TL	ST	TL/ST
3682	−310	−78.6	3.9	−246	−55	4.5	15.1	3.3	4.6
3800	251	30.5	8.2	187	27	6.9	15.7	2.9	5.4
3860	−310	−70.5	4.4	−306	−49	6.2	6.7	3.0	2.2
3944	167	41	4.1	113	10	11.3	11.2	3.2	3.5

Note. In the table, TL represents the response value of the transmission tower in the tower-line system, and ST represents the response value of the corresponding single tower. The minus sign stands for the compressive stress.

5.3.1. Comparison of the Wind-Induced Response of the Transmission Tower in the Tower-Line System and the Quasi-Static Response of the Corresponding Single-Tower under Different Wind Speeds. The results of the dynamic analysis of the tower in the tower-line system are compared with the quasi-static (QS) calculation results for the corresponding single tower under different wind speeds. A comparison of the displacements at the top of the tower is presented in Table 11. A comparison of the stress results of the tower members is provided in Table 12.

Tables 11 and 12 reveal that, under different wind speeds, the displacements at the top of the tower and the stress of tower members provided by the dynamic analysis of the tower-line system are greater than those of the quasi-static method for the corresponding single tower, demonstrating that coupling vibration between the transmission lines and the transmission tower occurs. This coupling effect increases both the lateral displacement of the tower and the axial compressive stress of the tower members. Therefore, the coupling vibration effect on the tower should be considered in the design of high-voltage transmission tower-line systems.

Because engineers are more concerned during the design process with the internal stress of the transmission tower members, to facilitate analysis, the ratio of the member stress of the tower by the dynamic analysis for the tower-line system and by the quasi-static (QS) calculation for the corresponding single-tower is defined as the dynamic amplifying coefficient, δ.

As evident from Table 12, when the wind speed is less than U_{10} = 18 m/s, at the tower bottom (0 m) and on the tower (a height of 19.8 m), the tower-line coupling effect increases with the wind speed. When the wind speed is greater than U_{10} = 18 m/s, δ decreases as the wind speed increases. When the wind speed reaches U_{10} = 19 m/s, the maximum axial compressive stress of the main member on compressive side of the tower bottom (0 m) reaches the design yield strength (310 MPa). When the wind speed reaches the design wind speed U_{10} = 25.3 m/s, the maximum compressive stress of more members reaches or exceeds the yield strength (310 MPa). At still higher wind speeds, δ decreases with increasing wind speed, likely because of the redistribution of the stress after the members yield. As the wind speed

Table 11: Comparison of the displacements of the tower calculated by dynamic analysis in the tower-line system and the displacement given by the quasi-static calculations for the corresponding single tower.

Wind speed	Node number	Displacement in the x-direction (m)			Displacement in the z-direction (m)		
		TL	QS	TL/QS	TL	QS	TL/QS
U_{10} = 14 m/s	727	0.091	0.071	1.28	−0.053	0.001	−53
	660	0.070	0.055	1.27	−0.032	0.0002	−160
U_{10} = 16 m/s	727	0.123	0.093	1.32	0.059	0.001	59
	660	0.096	0.072	1.33	0.036	0.0004	90
U_{10} = 17 m/s	727	0.145	0.105	1.38	0.080	0.001	80
	660	0.112	0.081	1.38	0.050	0.001	50
U_{10} = 18 m/s	727	0.170	0.117	1.45	0.102	0.001	102
	660	0.133	0.091	1.46	−0.062	0.001	−62
U_{10} = 19 m/s	727	0.202	0.131	1.54	−0.100	0.001	−100
	660	0.157	0.102	1.54	−0.062	0.001	−62
U_{10} = 20 m/s	727	0.192	0.145	1.32	0.116	0.001	116
	660	0.150	0.113	1.33	0.070	0.001	70
U_{10} = 21 m/s	727	0.221	0.160	1.38	0.096	0.002	48
	660	0.172	0.124	1.39	0.061	0.001	61
U_{10} = 22 m/s	727	0.258	0.175	1.47	−0.211	0.002	−105.5
	660	0.201	0.136	1.48	−0.129	0.001	−129
U_{10} = 23 m/s	727	0.286	0.186	1.54	−0.185	0.002	−92.5
	660	0.223	0.144	1.55	−0.116	0.001	−116
U_{10} = 24 m/s	727	0.301	0.202	1.49	−0.241	0.002	−120.5
	660	0.235	0.157	1.50	−0.151	0.002	−75.5
U_{10} = 25.3 m/s	727	0.426	0.225	1.89	−0.271	0.002	−135.5
	660	0.334	0.175	1.91	−0.168	0.002	−84

Note. In the table, TL represents the dynamic calculation results of the tower in the tower-line system, and QS represents the quasi-static calculation results as stipulated by the design code for the corresponding single tower.

increases, the stress of the main members by the quasi-static analysis continues to increase but remains within the elastic range. However, according to the dynamic time history analysis results, the stress of the corresponding members in tower-line system approaches or has already reached the material yield strength, and thus the range of stress increase is relatively small. Therefore, δ will decrease as the wind speed increases. Moreover, the stress distribution of the tower will result in the yielding of more members, especially the members near the tower bottom (0 m). For these reasons, δ for the tower bottom (0 m) will decrease further compared with that on the upper tower (e.g., height of 19.8 m).

In engineering design, the actual stress of main members plays decisive role. When the wind speed, U_{10}, increases from 14 to 18 m/s, even though the increasing magnitude of the stress of the main members caused by the coupling vibration effect in the tower-line system is pronounced (the corresponding δ value changes from 1.19 to 1.48), Table 12 indicates that the stress remains within the elastic range; that is, the tower remains safe. In such circumstances, even if the design is still based on the quasi-static method in the current design code, the results remain safe. When the wind speed is in the range of U_{10} = 19 to 25.3 m/s, the absolute value of the member stress caused by the effects of the tower-line coupling vibration is high (the corresponding δ value is between 1.39 and 1.06). The stresses of some main members are approaching or have already reached the material yield strength, whereas the absolute stress values calculated by the quasi-static method stipulated in the design code show that the members remain within the elastic range. Therefore, the tower-line coupled vibration effect will cause the stress of the main members in the transmission tower to reach the material yield strength, even if the wind speed is lower than the design wind speed. In such circumstances, the design based on the quasi-static analysis method in the current design code is not safe. In other words, the transmission tower designed in accordance with the existing quasi-static method stipulated in the current design code can only nominally withstand the wind load equivalent to that of the design wind speed (i.e., U_{10} = 25.3 m/s), but in practice it can only withstand wind loads that are less than that of the design wind speed (i.e., U_{10} < 25.3 m/s).

Because the quasi-static analysis method in the current design codes is relatively simple, it is easy for designers to follow. Therefore, based on the present results, when designing transmission towers, to accommodate the adverse effects of tower-line coupling vibration, the results given by the quasi-static method in design code should simply be multiplied by the corresponding tower-line coupling effect dynamic amplifying coefficient, δ. As indicated in Table 12,

Table 12: Comparison of the stress at the top of the tower calculated by dynamic analysis in the tower-line system and by the quasi-static calculation for the corresponding single tower.

Wind speed	Distance from the tower bottom (m)	Element number	Axial compressive stress of the main members of the transmission tower (MPa)		
			TL	QS	δ = TL/QS
U_{10} = 14 m/s	0	3682	183.19	154.59	1.19
	9	3273	154.57	128.84	1.20
	15	2994	106.71	88.53	1.21
	19.8	2991	152.40	126.47	1.21
	23.4	2882	97.46	78.96	1.23
	25.8	2880	115.32	92.15	1.25
U_{10} = 16 m/s	0	3682	221.35	179.40	1.23
	9	3273	187.72	150.63	1.25
	15	2994	131.50	104.96	1.25
	19.8	2991	185.81	148.35	1.25
	23.4	2882	121.75	94.06	1.29
	25.8	2880	145.17	109.63	1.32
U_{10} = 17 m/s	0	3682	259.80	193.05	1.35
	9	3273	222.67	162.63	1.37
	15	2994	157.27	114.00	1.38
	19.8	2991	222.00	160.40	1.38
	23.4	2882	147.30	102.36	1.44
	25.8	2880	177.26	119.25	1.49
U_{10} = 18 m/s	0	3682	306.27	207.47	1.48
	9	3273	262.84	175.31	1.50
	15	2994	187.08	123.55	1.51
	19.8	2991	262.94	173.13	1.52
	23.4	2882	176.51	111.11	1.59
	25.8	2880	214.15	129.40	1.65
U_{10} = 19 m/s	0	3682	310.00	222.94	1.39
	9	3273	265.24	188.91	1.40
	15	2994	189.66	133.79	1.42
	19.8	2991	263.83	186.79	1.41
	23.4	2882	175.59	120.47	1.46
	25.8	2880	206.87	140.27	1.47
U_{10} = 20 m/s	0	3682	310.01	239.17	1.30
	9	3273	276.54	203.18	1.36
	15	2994	197.09	144.52	1.36
	19.8	2991	276.08	201.12	1.37
	23.4	2882	185.27	130.29	1.42
	25.8	2880	225.51	151.67	1.49
U_{10} = 21 m/s	0	3682	310.02	256.14	1.21
	9	3273	288.76	218.12	1.32
	15	2994	206.41	155.75	1.33
	19.8	2991	288.17	216.12	1.33
	23.4	2882	192.63	140.53	1.37
	25.8	2880	232.08	163.58	1.42

Table 12: Continued.

Wind speed	Distance from the tower bottom (m)	Element number	Axial compressive stress of the main members of the transmission tower (MPa)		
			TL	QS	δ = TL/QS
U_{10} = 22 m/s	0	3682	310.12	273.53	1.13
	9	3273	310.05	233.45	1.33
	15	2994	258.15	167.26	1.54
	19.8	2991	310.03	231.52	1.34
	23.4	2882	240.35	150.99	1.59
	25.8	2880	289.32	175.70	1.65
U_{10} = 23 m/s	0	3682	310.18	286.04	1.08
	9	3273	310.11	244.57	1.27
	15	2994	280.94	175.59	1.60
	19.8	2991	310.07	242.66	1.28
	23.4	2882	265.35	158.47	1.67
	25.8	2880	304.39	184.38	1.65
U_{10} = 24 m/s	0	3682	310.18	290.20	1.07
	9	3273	310.11	261.25	1.19
	15	2994	281.28	188.10	1.50
	19.8	2991	310.07	259.40	1.20
	23.4	2882	271.52	169.82	1.60
	25.8	2880	307.75	197.60	1.56
U_{10} = 25.3 m/s	0	3682	311.69	294.05	1.06
	9	3273	310.74	284.45	1.09
	15	2994	310.07	205.48	1.51
	19.8	2991	310.47	282.72	1.10
	23.4	2882	310.00	185.53	1.67
	25.8	2880	304.34	215.91	1.41

Note. In the table, TL represents the dynamic calculation results for the tower in the tower-line system, and QS represents the quasi-static calculation results as stipulated by the design code for the corresponding single tower.

for example, under the designing wind speed (U_{10} = 25.3 m/s), from the bottom to the top of the tower, the δ value is 1.06, 1.09, 1.51, 1.10, 1.67, and 1.41, corresponding to the tower members at heights of 0, 9, 15, 19.8, 23.4, and 25.8 m, respectively. Because the absolute stress value of the members near the tower bottom is large, it is the controlling stress of the design. Therefore, to meet these requirements, the quasi-static analysis result of the whole tower must be multiplied by the tower-line coupling effect dynamic amplifying coefficient, δ (e.g., $\delta \geq 1.06$), at the bottom of the tower.

5.3.2. Comparison of the Wind-Induced Response of the Transmission Tower in the Tower-Line System and the Quasi-Static Response of the Corresponding Single Tower under Different Wind Directions. In the actual environment, different angles exist between the directions of the transmission lines and the wind. To analyze the influence of these different wind directions on the stress of the main members of the tower, in this section, based on two engineering cases where the wind speed, U_{10}, is 20 m/s and 25.3 m/s, the axial compressive stresses of the main members (see Table 12) are calculated using the dynamic analysis of the tower-line system under different wind direction angles (i.e., 90, 60, 45, and 0 degrees). The results are shown in Figure 25. As the wind direction angle increases, the axial compressive stress of the main members of the tower also increases. Therefore, the 90-degree wind angle creates the most adverse effects.

Because the members near the tower bottom (see Table 12) are usually dominant in design, the changes of the tower-line coupling effect dynamic amplifying coefficient, δ, under different wind directions (i.e., 90, 60, and 45) are also shown in Figure 26. As the wind direction angle decreases, δ also decreases, thus indicating that the amplifying effect of the tower-line coupling vibration is weakened. Overall, as the wind speed increases, the δ value curve develops, following a folding line-like pattern. However, at the design wind speed U_{10} = 25.3 m/s, the δ values corresponding to the three wind directions are approximately equal, indicating that the tower-line coupling effect dynamic amplifying coefficient, δ, is more sensitive to wind speed changes. Therefore, the actual engineering design can be safely completed assuming a wind direction angle of 90 degrees.

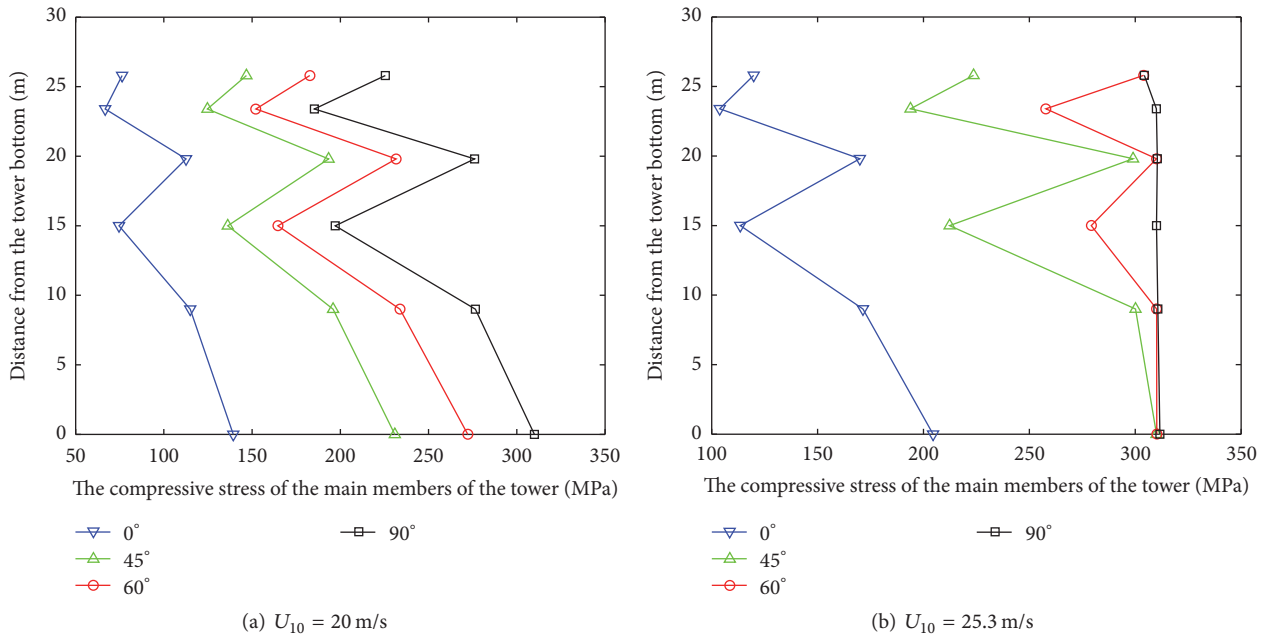

Figure 25: Comparison of the axial compressive stress of the main members of the tower in the tower-line system calculated using dynamic analysis under different wind directions.

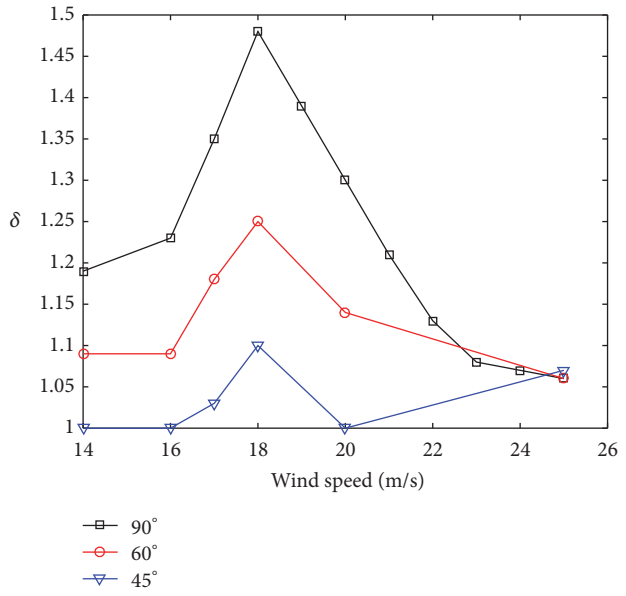

Figure 26: Comparison of the δ results of the members near the tower bottom under different wind speeds and wind directions.

6. Conclusions

In this study, a finite element model for transmission tower-line systems is established based on actual high-voltage transmission lines in East China. The wind-induced vibration responses of the tower-line system are analyzed using the established finite element model, and the accuracy of the finite element model is verified by comparing the results with field measurements. Based on the wind speed and wind pressure conversion theory and the modified *Davenport* spectrum, the wind load time history is simulated. The dynamic responses of the transmission tower in the tower-line system under different wind speeds and directions are analyzed, and the results are compared with those calculated using the quasi-static method stipulated in China's "Technical Codes for Designing 110 kV–750 kV Overhead Transmission Lines" (GB50545-2010) for the corresponding single tower. The following are the main conclusions drawn from this study:

(1) The coupling effect between the transmission lines and the transmission tower is an intrinsic property

of the tower-line system. When the transmission tower-line vibrates freely as a whole system, the fundamental natural frequency of the tower is much less than that of the corresponding single tower in the corresponding direction, and the overall vibrations of the tower and the lines are characterized by low frequencies and dense modes.

(2) Wind speed plays an important role in the tower-line coupling effect. The wind-induced vibration of the transmission tower in the tower-line system is more complicated than that in the single tower because of the coupling effect. Under the low wind speed, the coupling effect is less obvious and can be neglected. However, under the strong wind speed (i.e., the average wind speed at a height of 10 m is greater than 10.8 m/s, corresponding to a Beaufort number greater than 6), the coupling effect on the responses of the tower gradually becomes prominent, possibly resulting in the risk of premature failure of the tower-line system.

(3) Under the same design wind speed, the stress of the main members of the tower in the tower-line system increases more than that of the single tower. The maximum stress of the multiple members approaches or reaches the design yield strength of the steel. However, in the corresponding single tower, the stress of the members is much less than the design yield strength of the steel, and the tower remains safe. Under the same design wind speed, the member stress increase in the tower-line system is mainly caused by the vibration of the transmission lines due to the coupling effect, whereas the stress increase in the single tower is mainly caused by its self-vibration.

(4) Under a 90-degree wind of varying speeds, the displacement of the tower top and the stress of the main members are greater than the results of the quasi-static analysis for the corresponding single tower, demonstrating that the amplifying effect of dynamic coupling on the response of the transmission tower cannot be neglected in the tower-line system. The member stress in the tower decreases as the wind direction angle decreases, thus indicating that the wind direction angle of 90 degrees (perpendicular to the direction of the transmission lines) is the most adverse wind direction.

(5) The designs based on the quasi-static method stipulated in the current design code are unsafe because of the ignorance of the adverse impacts of coupling vibration on the transmission towers. In practical engineering, when the quasi-static method in the specifications is still used, the internal forces of the tower members given by the quasi-static analysis under the design wind speed can simply be multiplied by the tower-line coupling effect dynamic amplifying coefficient, δ, to approximate the adverse effects of the tower-line coupling on the transmission tower. For instance, the recommended value of δ is ≥ 1.06 based on the design parameters of the tower-line system presented in this paper. Accordingly, the cross-section of the tower members should be designed based on the internal stress adjusted by using the amplifying coefficient to ensure the safety of the tower.

Conflicts of Interest

The authors declare that there are no conflicts of interest regarding the publication of this paper.

Acknowledgments

This research has been funded by the National Natural Science Foundation of China (Grants nos. 51578512 and 51108425) and Outstanding Young Talent Research Fund of Zhengzhou University (Grant no. 1521322004).

References

[1] R. C. Battista, R. S. Rodrigues, and M. S. Pfeil, "Dynamic behavior and stability of transmission line towers under wind forces," *Journal of Wind Engineering & Industrial Aerodynamics*, vol. 91, no. 8, pp. 1051–1067, 2003.

[2] Q. Xie and J. Li, "Current situation of natural disaster in electric power system and countermeasures," *Journal of Natural Disasters*, vol. 15, no. 4, pp. 126–131, 2006.

[3] G. F. Zhao, *Research on Wind Induced Nonlinear Vibration of High Voltage Transmission Tower-Line Coupling System*, Tongji University, Shanghai, China, 2009.

[4] A. Hamada and A. A. El Damatty, "Behaviour of guyed transmission line structures under tornado wind loading," *Computers & Structures*, vol. 89, no. 11-12, pp. 986–1003, 2011.

[5] J. E. Mills, X. Ma, and Y. Zhuge, "Experimental study on multi-panel retrofitted steel transmission towers," *Journal of Constructional Steel Research*, vol. 78, pp. 58–67, 2012.

[6] Z. Yan, J. E. Mills, and X. Ma, "Modeling of steel lattice tower angle legs reinforced for increased load capacity," *Engineering Structures*, vol. 43, no. 10, pp. 160–168, 2012.

[7] C. Lu, X. Ma, and J. E. Mills, "The structural effect of bolted splices on retrofitted transmission tower angle members," *Journal of Constructional Steel Research*, vol. 95, pp. 263–278, 2014.

[8] C. Lu, X. Ma, and J. E. Mills, "Modeling of retrofitted steel transmission towers," *Journal of Constructional Steel Research*, vol. 112, pp. 138–154, 2015.

[9] H. Aboshosha, A. Elawady, A. El Ansary, and A. El Damatty, "Review on dynamic and quasi-static buffeting response of transmission lines under synoptic and non-synoptic winds," *Engineering Structures*, vol. 112, pp. 23–46, 2016.

[10] T. P. Boudreaux, "Hurricane Carla vs. Transmission Lines," *Civil Engineering & Construction Review*, pp. 70–72, 1962.

[11] H. S. Saffir, "Hurricane Hugo and Implications for Design Professionals and Code-Writing Authorities," *Journal of Coastal Research*, vol. 8, pp. 25–32, 1991.

[12] http://news.sina.com.cn/c/2009-11-17/152816622701s.shtml.

[13] K. R. Cooper, "Wind tunnel and theoretical investigations into the aerodynamic stability of smooth and stranded twin-bundled power conductors," Tech. Rep., National Research Council of Canada, 1973.

[14] A. M. Loredo-Souza and A. G. Davenport, "Wind tunnel aeroelastic studies on the behaviour of two parallel cables," *Journal of Wind Engineering & Industrial Aerodynamics*, vol. 90, no. 4-5, pp. 407–414, 2002.

[15] H. Z. Deng, S. Y. Zhu, X. M. Chen, and Z. M. Wang, "Wind tunnel investigation on model of long span transmission line system," *Journal of Tongji University (natural science)*, vol. 31, no. 2, pp. 132–137, 2003.

[16] Y. Guo, B. N. Sun, Y. Ye, G. H. Shen, and W. J. Lou, "Wind tunnel test on aeroelastic model of long span transmission line system," *Journal of Zhejiang University (Engineering Science)*, vol. 41, no. 9, pp. 1482–1486, 2007 (Chinese).

[17] F. Cluni, V. Gusella, and G. Bartoli, "Wind tunnel scale model testing of suspended cables and numerical comparison," *Journal of Wind Engineering & Industrial Aerodynamics*, vol. 96, no. 6-7, pp. 1134–1140, 2008.

[18] Z.-P. Liang and Z.-L. Li, "An aeroelastic model design of ultra-high voltage power transmission line systems," *Chongqing Daxue Xuebao/Journal of Chongqing University*, vol. 32, no. 2, pp. 131–136, 2009.

[19] G. Zhao, Q. Xie, S. Liang, and J. Li, "Wind tunnel test on wind-induced response of transmission tower and tower line coupling system," *Jianzhu Jiegou Xuebao/Journal of Building Structures*, vol. 31, no. 2, pp. 69–77, 2010.

[20] M. Takeuchi, J. Maeda, and N. Ishida, "Aerodynamic damping properties of two transmission towers estimated by combining several identification methods," *Journal of Wind Engineering & Industrial Aerodynamics*, vol. 98, no. 12, pp. 872–880, 2010.

[21] Q. Xie, C.-Y. Yan, and Y. Zhang, "Experiment and analysis on wind-induced dynamic tension of ice covered UHV conductors," *Gaodianya Jishu/High Voltage Engineering*, vol. 36, no. 8, pp. 1865–1870, 2010.

[22] Y. M. Desai, P. Yu, N. Popplewell, and A. H. Shah, "Finite element modelling of transmission line galloping," *Computers & Structures*, vol. 57, no. 3, pp. 407–420, 1995.

[23] G. H. Shen, G. H. Yuan, B. N. Sun, and W. J. Lou, "Dynamic impact effects on tower-line system due to Ice-shedding," *Engineering Mechanics*, vol. 27, no. 5, pp. 210–217, 2010.

[24] Y. Zhang, C. Yan, and Q. Xie, "Wind tunnel test on wind-induced dynamic responses of icing ultra high voltage transmission tower-line coupling system," *Zhongguo Dianji Gongcheng Xuebao/Proceedings of the Chinese Society of Electrical Engineering*, vol. 30, no. 28, pp. 94–99, 2010.

[25] F. Yang, J. Yang, and Z. Zhang, "Unbalanced tension analysis for UHV transmission towers in heavy icing areas," *Cold Regions Science and Technology*, vol. 70, pp. 132–140, 2012.

[26] L. Zhou, B. Yan, L. Zhang, and S. Zhou, "Study on galloping behavior of iced eight bundle conductor transmission lines," *Journal of Sound and Vibration*, vol. 362, pp. 85–110, 2016.

[27] M. J. He and B. F. Yang, "Site Vibration Experiment of Jiang Yin 500 kV Guyed Transmission Tower," *Structural Engineers*, no. 4, pp. 74–79, 2003.

[28] M. J. He, X. M. Yan, and Y. G. Zhang, "Synchronous test study of two adjacent transmission tower undergoing ambient excitation," *Journal of Vibration and Shock*, vol. 28, no. 11, pp. 155–158, 2009 (Chinese).

[29] Y. Momomura, H. Marukawa, T. Okamura, E. Hongo, and T. Ohkuma, "Full-scale measurements of wind-induced vibration of a transmission line system in a mountainous area," *Journal of Wind Engineering & Industrial Aerodynamics*, vol. 72, no. 1-3, pp. 241–252, 1997.

[30] H. Yasui, H. Marukawa, Y. Momomura, and T. Ohkuma, "Analytical study on wind-induced vibration of power transmission towers," *Journal of Wind Engineering & Industrial Aerodynamics*, vol. 83, pp. 431–441, 1999.

[31] M. Matsumoto, H. Shirato, T. Yagi, M. Goto, S. Sakai, and J. Ohya, "Field observation of the full-scale wind-induced cable vibration," *Journal of Wind Engineering & Industrial Aerodynamics*, vol. 91, no. 1-2, pp. 13–26, 2003.

[32] J. Li, Q. Yan, Q. Xie, and J. Chen, "Wind field measurements and wind-induced vibration responses of transmission tower during typhoon wipha," *Journal of Architecture & Civil Engineering*, vol. 26, no. 2, pp. 1–8, 2009.

[33] F. G. A. Al-Bermani and S. Kitipornchai, "Nonlinear analysis of transmission towers," *Engineering Structures*, vol. 14, no. 3, pp. 139–151, 1992.

[34] F. Gani and F. Légeron, "Dynamic response of transmission lines guyed towers under wind loading," *Canadian Journal of Civil Engineering*, vol. 37, no. 3, pp. 450–464, 2010.

[35] G. McClure and M. Lapointe, "Modeling the structural dynamic response of overhead transmission lines," *Computers & Structures*, vol. 81, no. 8–11, pp. 825–834, 2003.

[36] N. Prasad Rao and V. Kalyanaraman, "Non-linear behaviour of lattice panel of angle towers," *Journal of Constructional Steel Research*, vol. 57, no. 12, pp. 1337–1357, 2001.

[37] C. Klinger, M. Mehdianpour, D. Klingbeil, D. Bettge, R. Häcker, and W. Baer, "Failure analysis on collapsed towers of overhead electrical lines in the region Münsterland (Germany) 2005," *Engineering Failure Analysis*, vol. 18, no. 7, pp. 1873–1883, 2011.

[38] H. J. Dagher and Q. Lu, "System reliability analysis of transmission lines," *Engineering Structures*, vol. 15, no. 4, pp. 251–258, 1993.

[39] GB50545, *Technical Codes for Designing 110 kV–750 kV Overhead Transmission Lines*, National Standard of P.R. China, Planning Press, Beijing, China, 2010.

[40] L. L. Zhang, *Research on Wind Stochastic Field and Analysis of Dynamic Reliability for High-Rise Building with Wind Loading*, Tongji University, Shanghai, China, 2006.

[41] Q. G. Fei, Y. L. Xu, C. L. Ng, K. Y. Wong, W. Y. Chan, and K. L. Man, "Structural health monitoring oriented finite element model of Tsing Ma bridge tower," *nternational Journal of Structural Stability & Dynamics*, vol. 7, no. 4, pp. 647–668, 2007.

[42] C. Dyrbye and S. O. Hansen, *Wind Loads on Structures*, John Wiley & Sons, 1996.

[43] E. Simiu and R. H. Scanlan, *Wind Effects on Structures*, John Wiley & Sons, 1986.

[44] GB50012, *Load Code for the Design of Building Structures*, National Standard of P.R. China, Architecture & Building Press, Beijing, China, 2012.